

Article

Classifying Effluxable Versus Non-Effluxable Compounds Using a Permeability Threshold Based on Fundamental Energy Constraints

Soné Kotze ¹, Kai-Uwe Goss ^{1,2} and Andrea Ebert ^{1,*}

¹ Department of Computational Biology and Chemistry, Helmholtz Centre for Environmental Research (UFZ), Permoserstraße 15, 04318 Leipzig, Germany

² Institute of Chemistry, University of Halle-Wittenberg, Kurt-Mothes-Straße 2, 06120 Halle, Germany

* Correspondence: andrea.ebert@ufz.de

Abstract

Background/Objectives: Predicting whether a compound is subject to active transport is crucial in drug development. We propose a simple threshold for passive membrane permeability (P_m), derived from the cell's energy limitation, to identify compounds unlikely to be actively effluxed. **Results:** By considering fundamental cellular energy constraints, our approach provides a mechanistic rationale for why compounds with very high passive permeability in combination with low applied concentration will not undergo active efflux. This moves beyond the empirical observation (such as in previous systems that associate fast-permeating, poorly soluble compounds with low transporter activity) by grounding the prediction in the cell's energetic limitations. For MDCK (Madin–Darby canine kidney) cells, this threshold—normalized to the applied compound concentration (C_{ext})—was determined to be $P_m \times C_{ext} = 10^{-1.7}$ cm/s $\times \mu\text{M}$. **Methods:** To derive this threshold, we conducted an extensive analysis of literature-reported efflux ratios (ERs) in MDCKII cells overexpressing efflux transporters (MDR1, BCRP, MRP2; 294 datapoints across 136 unique compounds). Concentration-dependent measurements for Amprenavir, Eletriptan, Loperamide, and Quinidine—chosen because these borderline compounds exhibited the highest $P_m \times C_{ext}$ while still being actively effluxed—enabled the most accurate determination of the threshold. Literature ER values were re-evaluated through the experimental determination of reliable P_m values, as well as newly measured ER values with MDCK efflux assays. **Conclusions:** The results of these assays and the re-evaluation allowed us to reclassify all but three outliers (compounds with $ER > 2.5$ and $\log(P_m \times C_{ext}) > -1.7$). In contrast, more than 60% of the compounds analyzed without significant ER values (123 compounds) fell above the threshold, in strong agreement with our theory of an energy limitation to active transport. This permeability threshold thus provides a simple and broadly applicable criterion to identify compounds for which active efflux is energetically not feasible and may serve as a practical tool for early drug discovery and optimization, pending further validation in practical applications.



Academic Editor: René Holm

Received: 7 October 2025

Revised: 30 October 2025

Accepted: 5 November 2025

Published: 11 November 2025

Citation: Kotze, S.; Goss, K.-U.; Ebert, A. Classifying Effluxable Versus Non-Effluxable Compounds Using a Permeability Threshold Based on Fundamental Energy Constraints. *Pharmaceutics* **2025**, *17*, 1455. <https://doi.org/10.3390/pharmaceutics17111455>

Copyright: © 2025 by the authors.

Licensee MDPI, Basel, Switzerland.

This article is an open access article distributed under the terms and conditions of the Creative Commons Attribution (CC BY) license (<https://creativecommons.org/licenses/by/4.0/>).

Keywords: passive permeability; P-glycoprotein; active transport; efflux ratio; energy limit; MDCK

1. Introduction

Transport across biological membranes significantly influences the pharmacokinetic and toxicokinetic properties of drugs. Understanding active transport—especially efflux

mechanisms—is essential, as these processes greatly impact a compound's bioavailability, toxicity, and therapeutic efficacy [1]. Active transport of molecules through cell membranes functions in parallel with passive diffusion; however, instead of being driven by concentration gradients, active transport is energy-dependent and can occur against such gradients. As passive membrane permeability increases for more hydrophobic chemicals, more energy is needed for their active transport to counteract their rate of passive diffusion. Given that cells have a limited energy budget, this work sets out to prove the existence of a membrane permeability threshold beyond which active transport of molecules is no longer energetically viable.

Efflux proteins located in the apical membrane such as P-glycoprotein/multi-drug resistant protein 1 (P-gp, MDR1), breast cancer resistance protein (BCRP) and multi-drug resistance associated protein 2 (MRP2) actively pump out foreign substances from cells, which may affect the efficacy of drug uptake [2,3]. Due to their role in decreasing the intracellular concentration of chemotherapeutic agents, the over-expression of such efflux proteins plays a significant role in the resistance of cancerous tissue to multiple drugs [4,5]. Given that P-gp overexpression is linked to multidrug-resistance (MDR)—which diminishes the efficacy of chemotherapeutics, antibiotics, and antivirals—there is a significant need for cost-effective, rapid methods to detect P-gp substrates. These methods could not only assist in predicting a compound's toxicity, bioavailability, and drug–drug interaction potential [6] but also enable the early exclusion of problematic candidates, thereby mitigating MDR-related challenges during drug discovery [7]. Therefore, it is of great importance in the pharmaceutical industry to ascertain whether drugs are affected by such efflux transporters. Traditionally, the passive membrane permeability (P_m) of a compound, as well as the involvement of efflux transporters—quantified using a metric known as the efflux ratio (ER)—is determined through bidirectional transport assays using epithelial cell lines such as MDCK or Caco-2. These assays have also been utilized to gather information on the chemical nature of efflux transporter substrates [8,9], in the hopes of enabling the development of predictive in silico models linking physicochemical properties to carrier-mediated efflux (i.e., QSAR models [10], machine learning [11,12]). However, the utility of such models is hindered by their limited interpretability, narrow chemical coverage due to limitation in the training datasets, as well as their reliance on inconsistent datasets.

Efforts have also been made to develop simple and fast interpretations of the molecular characteristics that define efflux substrates [13–17]. These studies seek to establish simple and broadly applicable “rules-of-thumb” for hit-to-lead optimization. It has been proposed that such simple rules might have a more significant impact compared to complex predictive models [6], although their limitations are well recognized, and the need for mechanism-based approaches has been emphasized [18,19]. In this study, we propose another simple and easily applicable, yet mechanistically based, rule-of-thumb: compounds exceeding a certain passive membrane permeability threshold are less likely to exhibit significant transporter-facilitated efflux. The objective of this work was to test this hypothesis and determine whether it could be translated into a guideline for the rapid separation of compounds that could exhibit significant transporter-facilitated efflux from those that cannot, based on their membrane permeability. The permeability-based separation proposed here does not differentiate between efflux substrates and non-substrates. Instead, it differentiates compounds whose ADME characteristics can be significantly affected by efflux transporters from those that cannot, irrespective of whether they are substrates. Establishing a permeability-based separation guideline could prove valuable for drug classification, or could assist in the rational direction of lead optimization towards desired efflux effects. Since it was shown recently by Dahley et al. [20] that the biological Caco-2/MDCK membrane permeability of drugs is well predicted by the solubility diffusion

model (SDM), permeability-based separation can in most cases be performed without the need for experimental assays. Furthermore, because this rule is based on a fundamental physical principle (the energy limit of the cell) it is not limited to P-gp, but should also apply to any efflux transporter that consumes ATP.

The aims of this study were to: (i) evaluate existing MDCKII ER data for MDR1, BCRP and MRP2, and establish a crude membrane permeability cut-off above which compounds appear to not be affected by active efflux. Compounds that seem to contradict this threshold can then be flagged as outliers and subsequently examined. Secondly, it was aimed (ii) to identify compounds located at or near the threshold for further investigation with concentration-dependent monolayer efflux assays. The resulting data can then be used to quantify the maximal flux rate (i.e., the maximum amount of compound that can be actively effluxed per unit time) and the corresponding energy limit. Finally, we aimed (iii) to link this energy limit with a specific P_m value and perform a sensitivity analysis to highlight the caveats and limitations associated with defining a rule-of-thumb P_m threshold.

2. Theory

2.1. Transport Model

As compounds permeate from one compartment to another across a cell layer, they encounter various resistances, both in series and in parallel. This includes aqueous boundary layers (ABL), as well as the cell layer itself, consisting of the basolateral and apical membranes, as well as the cytosol. The permeability (P) of each barrier is inversely proportional to its resistance. As is evident in Figure 1, the unidirectional active transport facilitated by P-gp (denoted as $P_{\text{pgp,app}}^{\text{active}}$) and a basolateral uptake transporter (denoted as $P_{\text{b,app}}^{\text{active}}$) occurs in parallel to the passive diffusion through the apical membrane ($P_{m,a}$) and the basolateral membrane ($P_{m,b}$), respectively. The in vitro situation during MDCK/Caco-2 assays is comparable to the in vivo scenario, save for the presence of a permeable filter on which cells are grown, as well as thicker unstirred water layers. A detailed description of the conceptual model used, as well as the various resistances and how they can be quantified, can be found in Kotze et al. [21].

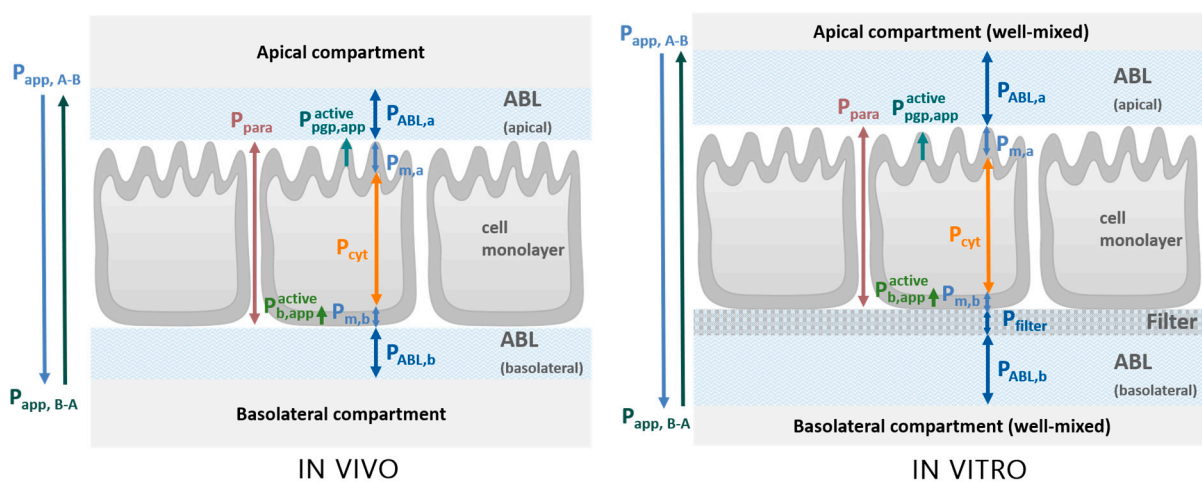


Figure 1. Schematic representation of permeation barriers in vivo and in vitro. In vivo (left), well-mixed donor and acceptor compartments are separated by the apical ABL, the cell monolayer, and the basolateral ABL. The in vitro system (right) additionally includes a filter layer and exhibits a thicker ABL (not to scale). Reproduced from Kotze et al. [21], licensed under CC BY 4.0. In the case of in vivo transport in intestinal cells for example, the apical compartment is the lumen of the gastrointestinal tract (GIT), and the basolateral compartment is the blood.

The total permeability through all barriers (as measured by transport assays) is referred to as the apparent permeability (P_{app}). Consequently, P_{app} , as a function of all individual permeabilities, can be broken down into the contributions from each component, enabling the separate evaluation and quantification of permeability through each layer (see Equations (S1) to (S8) in the Supplementary Materials S1 (Section S1) for modeled permeabilities and local compound concentrations as described in detail in Kotze et al. [21]).

2.2. Maximal Active Transport Flux and Borderline Compounds

It is crucial to distinguish between the two different threshold values discussed in this work: the maximal flux and the associated maximal passive membrane permeability. The maximal flux, or $J_{pgp,active}$, refers to the maximum moles of compound that can be actively transported by any transporter per unit area and time ($\mu\text{mol}/\text{cm}^2/\text{s}$) assuming the cell has limits to the energy it can invest in its transporters. The energy limit thus corresponds to the maximal $J_{pgp,active}$ possible given limited energy production of the cell. Both the value for the active efflux permeability $P_{pgp,app}^{active}$ (cm/s) facilitated by P-gp from the apical membrane as well as the actively transported flux $J_{pgp,active}$ at a given apical freely dissolved concentration can be extracted from model fits of experimental MDCK data. It is important to consider only the freely dissolved concentration because only this fraction can permeate the membrane. A theoretical calculation of the maximal possible $J_{pgp,active}$ based on the cell's ATP turnover can also be performed to compare with the empirical value as a plausibility check; see Supplementary Materials S1 (Section S2). However, $J_{pgp,active}$ is an impractical metric, since it is complex to determine and not meaningful for the average scientist. Thus, we aimed to ultimately link it with passive membrane permeability, P_m , which is usually readily available, or easily determinable if not. The P_m threshold is thus the specific passive membrane permeability value where the rate of passive influx of a chemical would require an active efflux rate that exceeds the cell's maximal $J_{pgp,active}$.

As such, chemicals with a P_m value above the threshold would be unlikely to show significant efflux, since their high permeability would impose an unsustainable energy demand on the cell. The link between $J_{pgp,active}$ and P_m arises from the assumption that almost all the compound passively diffusing into the cells is actively effluxed, which is a valid approximation for high efflux ratios. If membrane permeability poses the main passive resistance, passive influx corresponds to $P_m \times C_{ext}$. For significant ER values, the energy limit can thus be approximated by the applied concentration-corrected membrane permeability, $P_m \times C_{ext}$. Although concentrations in MDCK/Caco-2 efflux assays typically vary only within a narrow range (1–100 μM), therapeutic plasma concentrations span more than six orders of magnitude [22]. It is therefore essential to take C_{ext} into account when defining the threshold.

Since $J_{pgp,active}$ depends on several factors, the resultant $P_m \times C_{ext}$ threshold would not be a definite cut-off line. Rather, one could expect the existence of a transitional range of permeability values that separate compounds that cannot be effectively effluxed from those that can. For compounds that have a $P_m \times C_{ext}$ value within this window (which we designate as “borderline compounds”) concentration plays a particularly pivotal role. For such borderline compounds, we observed concentration-dependent saturation of active transport. The rationale is that at low concentrations, compounds can be efficiently effluxed without substantially straining the cell's energy budget. However, as the concentration increases, a larger quantity of the compound enters the cell, which brings the increased efflux closer to reaching the energy limit. Finally, at a certain higher concentration and beyond, the rate of passive permeation into the cell far exceeds the rate at which it can be effluxed, due to the depletion of the energy budget.

3. Material and Methods

3.1. Determination of Passive Membrane Permeability P_m

To determine the energy limit, a reliable P_m is needed. P_m can be determined experimentally, or predicted with in silico methods. The pH-partition hypothesis dictates that only the neutral fraction (f_n) of a chemical can traverse membranes by passive diffusion, because the permeability of the ionic fraction is negligible in comparison [23]. The P_m of ionizable chemicals is therefore dependent on pH, or the neutral fraction f_n :

$$P_m = P_0 \times f_n \quad (1)$$

The interconversion between the intrinsic permeability P_0 and P_m is straightforward when the neutral fraction is known. For all compounds in this study, pKa values were used to determine f_n at pH 7.4 according to Escher et al. [24]. Experimental pKa values were preferred; however, where no experimental pKa could be sourced, pKa values were instead determined using the software ACD/pKa GALAS from ACD/Percepta (version 2020.1.2, Advanced Chemistry Development, Inc. (ACD/Labs), Toronto, ON, Canada, www.acdlabs.com, accessed on 1 September 2025) [25]. For zwitterions, only the non-charged neutral species was assumed to permeate the membrane, and the respective fraction was calculated according to Ebert and Dahley [26]. See Tables S1–S3 in the Supplementary Materials S2 for details.

For epithelial cells such as the MDCK line used in this study, it is crucial to note that microvilli are created by the folded apical membrane. Consequently, it is believed to have a greater surface area compared to the basolateral membrane. If a difference in surface area indeed exists between the apical and basolateral membrane, it is suspected to have a significant effect on the resulting energy limit of this work. In our previous study we speculated that the factor of 24 [27] we routinely implemented to account for the greater apical membrane surface area was likely excessive [21]. As such, in the main text of this study we used a more conservative apical membrane surface area factor (SA) of 7.5 (determined specifically for MDCKII cells as the average value of these cells cultivated on different filters [28]), and compared this to the two other proposed factors of 24 and 1 on the extreme ends of the probable range in the Supplementary Materials S1 (Sections S9–S16). The factor of 1 naturally indicates that the surface areas between apical and basolateral membranes are identical.

3.1.1. In Silico Prediction of P_m Using UFZ-LSERD/COSMO-RS

Experimental P_m values are the most reliable, so for this work such values were preferred when available for a given compound. When no reliably extracted experimental P_0 value was available for the calculation of P_m , P_0 was estimated based on the solubility-diffusion model (SDM) by utilizing hexadecane as a model for the hydrocarbon core of the membrane [20,29]:

$$P_{0,SDM} = \frac{D_{hex} \times K_{hex/w}}{x_m} \quad (2)$$

where $K_{hex/w}$ is the hexadecane–water partition coefficient of the compound, D_{hex} is the diffusion coefficient of the compound in hexadecane, and x_m refers to the thickness of the hexadecane-like hydrocarbon core of the cell membrane. It is assumed that D_{hex} is one-tenth of D_w [29], and thus it was calculated based on the molecular weight of the compound, adjusted for the temperature of 37 °C (see Supplementary Materials S1 (Section S1)). The $K_{hex/w}$ was obtained from the LSER database [30]. $K_{hex/w}$ values determined from experimental descriptors were given precedence and duly categorized. In cases where experimental descriptors were not available, $K_{hex/w}$ values derived from calculated descriptors were utilized instead. For comparative purposes, $K_{hex/w}$ values

were also generated for all compounds using the quantum chemically based software COSMOtherm (version C30, release 18, COSMOlogic GmbH & Co. KG, Leverkusen, Germany, www.cosmologic.de, accessed on 30 September 2021) [31]. COSMOtherm values were only used for zwitterions, and compounds with a molecular weight > 1000 g/mol. The P_0 of the MDCK cell membrane $P_{0,MDCK}$ was subsequently calculated from $P_{0,SDM}$ based on the empirical correlation established by Dahley et al. [20]:

$$P_{0,MDCK} = 0.84 \log P_{0,SDM} - 1.85 \quad (3)$$

3.1.2. Experimental Determination of P_m with Bidirectional MDCK Assays

Membrane permeability P_m and the resultant P_0 values can also be determined with in vitro bidirectional assays. In this study, P_0 values for all compounds were preferentially sourced from our own experiments and from Ebert et al. [32], who extracted P_0 values from experimental Caco-2/MDCK P_{app} data from several sources while accounting for the many pitfalls associated with P_0 determination. Consequently, they are regarded as the most dependable P_0 values available.

3.1.3. Experimental Determination of P_m with PAMPA and SDM

Using hexadecane as the membrane in HDM-PAMPA (Parallel Artificial Membrane Permeability Assay) has been shown an effective way to determine reliable experimental $K_{hex/w}$ [33]. These $K_{hex/w}$ values could subsequently be applied via Equations (2) and (3) to calculate a P_m for MDCK cells that is more reliable than those generated from predicted $K_{hex/w}$ values [20]. For this work, HDM-PAMPA assays were performed for some compounds at suitable pH values. Detailed descriptions of the methodology used can be found in an accompanying study by Dahley et al. [33]. Further details about the experiments first reported in Dahley et al. [33] that are relevant to this study (including the chemicals and reagents used, the experimental conditions, the experimentally obtained P_{app} , P_0 and $K_{hex/w}$ values, as well as the resultant P_m values calculated from it, etc.) can be found in the Supplementary Materials S1 (Sections S3 and S4) and S2 (Tables S5 and S6).

3.2. Analysis of ER Data

3.2.1. Evaluation of ER Data from Literature

Three distinct datasets of ER values were compiled for substrates of P-gp, BCRP and MRP2, as these are the three most clinically relevant apically located efflux transporters. A literature search was conducted to identify compounds with an $ER \geq 2.5$ [34], measured using bidirectional MDCK transport assays. For compounds with ER values reported by multiple sources, all values were included in the analyses, even if some sources reported conflicting ER values below the threshold. A total of 294 datapoints were collected, representing 136 unique compounds, with the majority of the data coming from MDCKII-MDR1 assays, since assays for MDCK-BCRP and MRP2 are considerably less common. We note that this compilation is not exhaustive. MDCKII-MDR1 assay data from 24 different sources were used [34–57]. The dataset included 227 data points (i.e., ER values) from 107 distinct compounds. MDCK-BCRP assay data was obtained from 12 different sources [56,58–68]. The dataset contained 52 data points from 33 distinct compounds. MDCK-MRP2 assay data was obtained from 8 different sources [69–76]. The dataset contained 15 data points from 11 distinct compounds. A fourth, separate dataset was also curated for compounds with insignificant ER values below the cut-off line. For this, data was obtained from 4 sources [36,38–40]. This dataset comprised 125 datapoints representing 123 compounds. For all datasets, compounds with a permanent charge were excluded from subsequent analyses because they lack a neutral fraction capable of passively permeating through the hydrophobic core of the membrane.

The P_m for each compound was then calculated using Equation (1) and the corresponding applied concentrations used by the respective studies were noted and used to calculate the concentration-corrected P_m values ($P_m \times C_{ext}$). The MDCK ER values from the studies of all three transporters and the $P_m \times C_{ext}$ values determined for each respective compound are depicted in Figure 2. Tabulated values of Pgp/MDR1, BCRP and MRP2 substrates along with their chemical properties can be found in the Supplementary Materials 2 (Tables S1, S2 and S3, respectively), along with the concentration-corrected P_m values (Table S4).

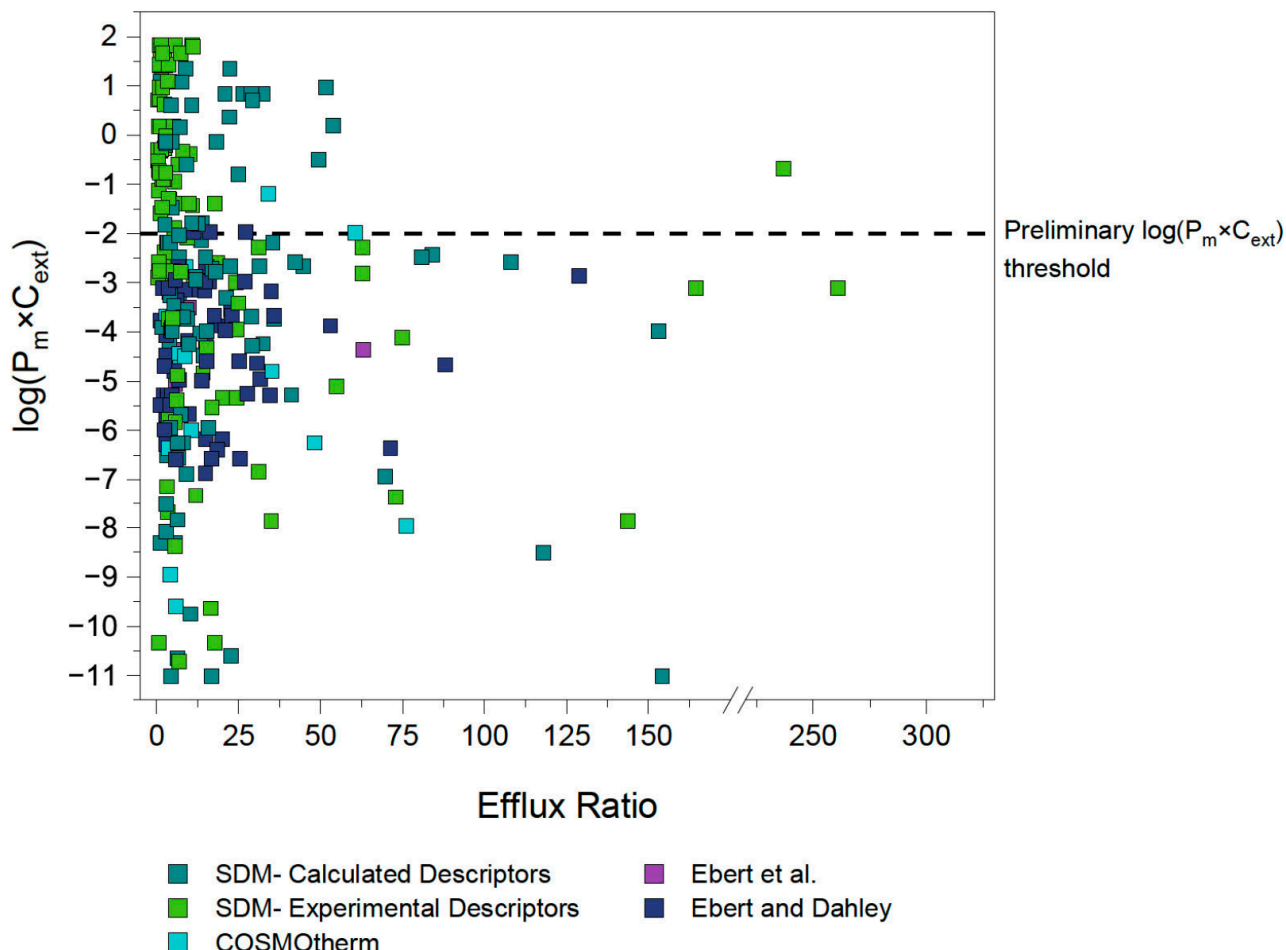


Figure 2. ER and $\log(P_m \times C)$ values of compounds shown to have significant (>2.5) ER values as determined with MDCK assays. All ER values sourced from literature for MDCKII-MDR1, -BCRP and -MRP2 bidirectional assays. Experimental P_m values sourced from Ebert et al. [32] and Ebert and Dahley [26] were preferred. If no experimental P_m values were available, P_m was calculated with the Solubility Diffusion Model (SDM) using $K_{hex/w}$ values determined preferably from experimental descriptors if available, and calculated descriptors if not. For zwitterions and compounds with MW > 1000 g/mol, COSMOtherm was used to calculate P_m .

3.2.2. Re-Determining the ER of Outlier Compounds with Bidirectional MDCK Assays Chemicals and Reagents

All chemicals and reagents can be found in the Supplementary Materials S1 (Section S3).

Cells and Cell Culture

MDCKII-MDR1 cells were obtained from The Netherlands Cancer Institute (Amsterdam, The Netherlands). The cell medium was Dulbecco's modified Eagle medium (DMEM) (1X) + GlutaMAX™-I supplemented with 10% fetal bovine serum (FBS), 100 U/mL peni-

cillin and 100 $\mu\text{g}/\text{mL}$ streptomycin. Cells were maintained at 37 °C in an atmosphere of 5% CO₂ and passaged twice a week.

Bidirectional MDCK Assays

MDCK bidirectional transport assays were performed as described in Kotze et al. [21,77]. MDCKII-MDR1 cells (passages 20–40) were seeded at a density of 1.5×10^5 cells/insert onto 12-well transwell inserts (CellQART, Northeim, Germany; pore size: 0.4 μm ; filter thickness: 11.5 μm , porosity: 100×10^6 pores/cm²). After seeding, cells were maintained as outlined in Cells and Cell Culture Section and grown for 4 days. The day prior to the experiment, the cell medium was refreshed. The transport buffer was HBSS and HEPES with a pH of 7.4. Stock solutions were prepared in the transport buffer. Prior to the experiment, the pH of the stock solutions and buffer was controlled with a Rapid_pH™ Automated pH Meter (Hudson Robotics, Inc., Springfield, NJ, USA), as was the pH of all samples after the conclusion of the experiment. Inserts were placed in 12-well plates from TPP Techno Plastic Products AG (Trasadingen, Switzerland). Sampling was conducted at 3 to 4 time intervals, with the duration tailored specifically for each compound and measurement direction to guarantee sink conditions. In between sampling steps, plates were placed in a Titramax and Inkubator 1000 orbital shaking incubator from Heidolph Instruments GmbH & Co. (Schwabach, Germany) at 450 rpm and 37 °C. At the final sampling step, the donor compartment was sampled for mass balance calculations. For each insert, the trans-epithelial electrical resistance (TEER) across the cell monolayer was measured at 37 °C using an EVOM epithelial tissue volt/ohmmeter (World Precision Instruments Inc., Sarasota, FL, USA) before and after the experiment to ensure that cell monolayer remained intact throughout the experiment. Lucifer yellow (LY) was utilized as a paracellular marker to further confirm the integrity of the cell monolayer. For this, the LY permeability of each insert was assessed post-experiment by measuring the fluorescence intensity (excitation: 485 nm, emission: 538 nm) in samples from the basolateral compartment using a SpectraMAX Gemini EM spectrophotometer (Molecular Devices LLC., San Jose, CA, USA). Inserts that demonstrated a LY permeability greater than the pre-defined threshold of 1.5×10^6 cm/s were excluded [78], unless their P_{app} results were qualitatively consistent with those of replicate inserts that fell within the LY threshold.

Samples were analyzed with an Infinity II 1260 LC system coupled with a 6420 triple quadrupole 145 with ESI source (Agilent Technologies Inc., Santa Clara, CA, USA). Either a Kinetex® F5 (2.6 μm ; 100 Å; 50 × 3.0 mm) or C18 (2.6 μm ; 100 Å; 50 × 3.0 mm) LC column was used (Phenomenex Inc., Torrance, CA, USA). P_{app} was calculated from acceptor compartment concentrations as described in Kotze et al. [21]. P_{app} values at each time point were corrected using the calculated recovery, as done by Neuhoff [79]. The data is shown as the mean of the recovery-corrected P_{app} ± standard deviation from at least two samples from each replicate. To account for lag time [80] the first time point in the A → B direction was excluded. The ER was determined as the ratio of the mean P_{app} values in the B → A direction and A → B direction according to:

$$\text{ER} \equiv \frac{J_{B \rightarrow A}}{J_{A \rightarrow B}} \equiv \frac{P_{app,B \rightarrow A}}{P_{app,A \rightarrow B}} \quad (4)$$

3.2.3. Concentration-Dependent MDCK Assays for Borderline Compounds

Bidirectional MDCK-MDR1 assays were performed as described in Bidirectional MDCK Assays Section and Kotze et al. [21] to determine P_{app} values as well as the ER using stock solutions with varying concentrations. Concentrations were selected to cover the range of viable concentrations within the boundaries of the experimental protocol and LC-MS quantification. When DMSO was necessary for solubility, the total concentration

was maintained at a maximum of 0.1%, and the transport buffer was supplemented with the same concentration to avoid the creation of a DMSO gradient across compartments. MDCK assays conducted for this section were performed in triplicate, with sampling occurring at four consistent time intervals. The data from these assays are presented as the mean of the recovery-corrected P_{app} \pm standard deviation from at least three samples from each replicate.

3.2.4. Determination of $P_{pgp,app}^{active}$ and Maximal Flux $J_{pgp,active}$

The recovery-corrected $A \rightarrow B$ and $B \rightarrow A$ permeabilities determined for each concentration of the assays in Section 3.2.3 were used in the evaluation of the saturation experiments. The thickness of the apical and basolateral ABL, along with the thickness of the filter and its effective surface area, as well as the P_0 , D_w , D_{cyt} and pKa values for each compound were used to determine the permeability through the individual resistances (ABLs, membranes, cytosol and filter). The paracellular permeability was determined as described by Bittermann and Goss [29], with a factor of 0.1 applied to ensure that its final value matches the paracellular permeabilities generally observed for our MDCKII-MDR1 cell set-up [21]. Based on the compound's pKa values and the external pH, the external neutral fraction was calculated according to Escher et al. [24]. After determining the cytosolic pH as a function of the external pH according to Dahley et al. [20], the neutral fraction in the cytosol was similarly calculated.

The experimental P_{app} and known P_0 values were subsequently utilized to fit the apparent permeabilities facilitated by P-gp ($P_{pgp,app}^{active}$) and the basolateral uptake transporter ($P_{b,app}^{active}$). The fitting of $P_{app} A \rightarrow B$ (see Equation (S3)) was done for each concentration using the Excel SOLVER function which minimized the difference between the calculated and experimental apparent permeability by varying $P_{pgp,app}^{active}$. Using the starting concentrations ($\mu\text{mol L}^{-1}$), as well as the extracted $P_{pgp,app}^{active}$, it was possible to calculate the concentration of the compound adjacent to the apical membrane in the cytosol ($C_{cyt,a}$) (see Equation (S6)). The flux of actively transported compound, $J_{pgp,active}$, was then derived from the product of $P_{pgp,app}^{active}$ and $C_{cyt,a}$ in $\mu\text{mol cm}^{-2} \text{ s}^{-1}$. Ideally, a sequential calculation would have been performed: First, for the basolateral transporter $P_{b,app}^{active}$, by fitting the $B \rightarrow A$ permeability (see Equation (S4)) assuming that the apical membrane does not pose a significant resistance in this transport direction. Subsequently $P_{pgp,app}^{active}$ would be determined by fitting the $A \rightarrow B$ permeability. However, due to unexpected experimental effects, only $A \rightarrow B$ permeability could be fitted to determine $P_{pgp,app}^{active}$, under the assumption of insignificant basolateral active transport. This is elaborated upon and justified in the Supplementary Materials S1 (Section S7).

3.2.5. Linking the Maximal Flux Value with a Membrane Permeability Threshold

For the compounds that exhibited saturation effects in the concentration-dependent MDCK assays and therefore evidently reached the maximum flux plateau, classic non-linear Michaelis–Menten fits for extracted $J_{pgp,active}$ depending on $C_{cyt,a}$ were conducted with IGOR Pro 7 (WaveMetrics Inc., Lake Oswego, OR, USA) in order to ascertain the maximal $J_{pgp,active}$. The maximal $J_{pgp,active}$ was then used to calculate the corresponding threshold P_m value depending on ER (i.e., the highest passive membrane permeability a compound can have in order to potentially be subject to active efflux), again using the Excel solver function to optimize P_m for various $P_{pgp,app}^{active}$, minimizing $J_{pgp,active,max} - P_{pgp,app}^{active} \times C_{cyt,a}$. ER and $C_{cyt,a}$ were calculated using Equations (S5) and (S6), respectively. In contrast to our earlier assumption that nearly all compounds passively diffusing into the membrane are subsequently effluxed, this approach also allows determination of P_m for low ER values, where that assumption is not valid. In essence, P_m was back-calculated based on P-gp

activity, and in so doing, it was established what P_m value is possible for P-gp activity to equal the maximal flux value. Compound concentrations, paracellular transport and the apical membrane surface area were varied for the sensitivity analysis of the P_m threshold.

4. Results and Discussion

4.1. First Estimation of $P_m \times C_{ext}$ Limit

To validate our assumption of a $P_m \times C_{ext}$ limit for active transport, the efflux ratios for P-gp, BCRP and MRP2 substrates were extracted from literature as described in Section 3.2.1. Figure 2 shows the $P_m \times C_{ext}$ plotted against the reported efflux ratios for a total of 286 datapoints, representing 132 unique compounds (after exclusions, see details in Section 4.3). Different colors indicate the source of each P_m value, which in turn reflects the reliability of the experimental or predicted data.

A rough approximation for the cut-off value of compound permeability was defined to guide the initial investigations. This cut-off $P_m \times C_{ext}$ value was identified by evaluating the distribution of the data (Figure 2). Data points which had $P_m \times C_{ext}$ values based on the reliable P_0 values extracted by Ebert et al. [32] and Ebert and Dahley [26] were given particular weight. As a result, a preliminary threshold of $\log(P_m \times C_{ext}) = -2$ was set as an initial approximation of where the energy threshold (and therefore the associated membrane permeability threshold) could lie, as it can be observed that none of the reliable experimental $P_m \times C_{ext}$ values reported by Ebert et al. [32] exceed this value.

4.2. Identification and Investigation of Outliers

All 59 datapoints (41 compounds) with an ER ≥ 2.5 and with a $\log(P_m \times C_{ext}) > -2$ were thus identified as tentative outliers to our hypothesis, see Table S6. Owing to the specific threshold selection, all outliers had P_m values predicted from $K_{hex/w}$ values determined either with experimental or calculated descriptors. $K_{hex/w}$ values obtained from experimental descriptors are typically considered as quite reliable, suggesting that it was more likely that the reported ER values for these outliers were incorrect. Therefore, MDCK assays were conducted to determine the ER independently in an effort to replicate the findings of the original study. Only MDCKII-MDR1 assays were performed since only the MDR1 dataset had outliers in this category. In contrast, $K_{hex/w}$ values from calculated descriptors are deemed less reliable, so for the corresponding outliers it was assumed that the calculated P_m was false. HDM-PAMPA experiments were preferentially performed to obtain more reliable $K_{hex/w}$ values as already described in Section 3.1.3. Figure 3 presents a schematic summarizing the process used to determine how each outlier compound was probed. These assumptions served as a general guideline; however, for some compounds, both MDCK as well as HDM-PAMPA were eventually performed.

4.3. Outlier Reclassification

Figure 4 represents the collection, analysis and reclassification of the data. Five outlier compounds (gefitinib, lopinavir, ritonavir, zotepine and dasatinib) were excluded for exhibiting stability and solubility issues that precluded reliable PAMPA/MDCK assays. Notably, two-thirds of the MDR1 outlier compounds originated from just three of the 22 sources. Data obtained from Wager et al. [34] accounted for over 30% of the outliers. Furthermore, with the exception of one compound, every outlier reported by Wager et al. [34] was categorized under “Experimental Descriptors”, suggesting that the ER values (rather than the P_m) for these outliers are likely questionable. Significant ER values reported by Wager et al. as well as two other sources overrepresented in the outlier data—Obradovic et al. [43] and Wang et al. [81]—were frequently contradicted by other sources that reported no significant ER. As such, the values from these sources were approached with caution.

Accordingly, the 22 outliers from these sources were reclassified based on the contradictory non-significant ER values obtained from our own MDCK assays and/or from other sources. Two outliers were reclassified as non-outliers based on newly determined P_m values from PAMPA experiments. Ten outliers were reclassified as borderline compounds based on P_m values—often newly determined with PAMPA—that placed their $\log(P_m \times C)$ values between -2 and -1 . The outliers, their reclassification and the basis for it can be found in Table S6 of the Supplementary Materials. The results of the MDCK and PAMPA assays can be found in the Supplementary Materials S1 (Sections S4 and S5) as well as S2 (Table S5).

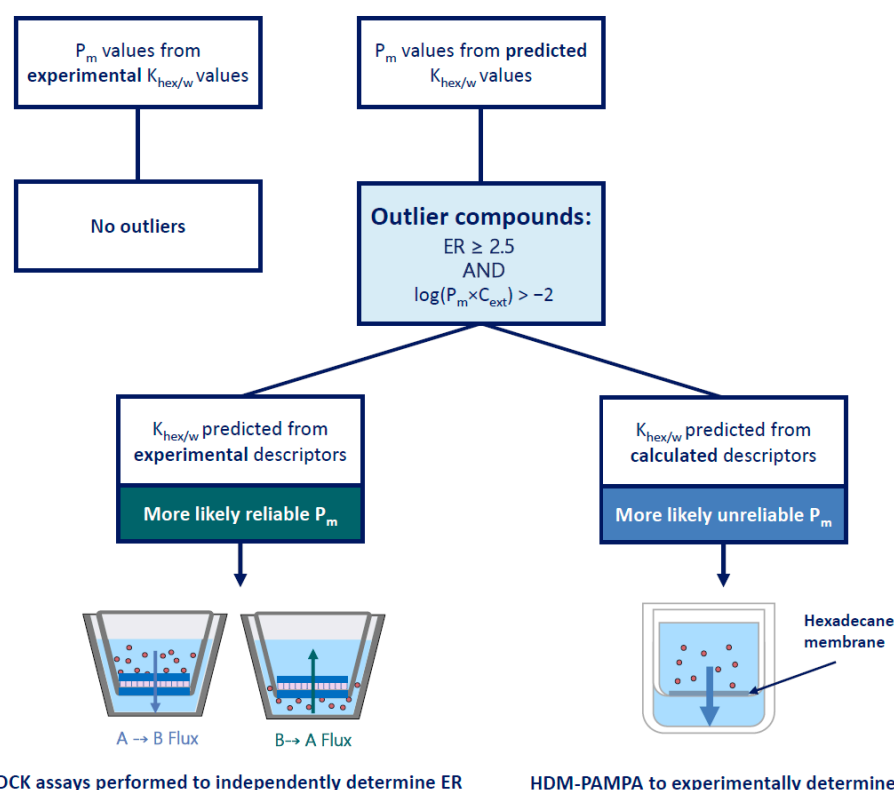


Figure 3. Schematic depicting the methodical experimental investigation of outlier compounds based on the assumed reliability of P_m values. All outlier compounds had P_m values determined from predicted $K_{hex/w}$ values. If the $K_{hex/w}$ was determined from experimental descriptors (reliable P_m values), MDCK assays would preferentially be performed to confirm the reported ER. If the $K_{hex/w}$ was determined from calculated descriptors (unreliable P_m values), HDM-PAMPA was preferentially performed to determine a reliable P_m based on experimental $K_{hex/w}$ values.

After evaluation, there are three remaining outliers: dextrorphan, mequitazine and terfenadine. Both dextrorphan and mequitazine have reported ER values (2.6 and 2.8, respectively) that barely surpass the significance threshold and are thus not very convincing outliers. For terfenadine, our own MDCK assays did find a significant, albeit also very low ER value of 2.8. Furthermore, a newly determined PAMPA $K_{hex/w}$ value for terfenadine confirmed a $\log(P_m \times C_{ext})$ value above the threshold, at 0.08. However, this compound exhibits very low recovery in the MDCK assays, which likely would have been the situation in assays from other sources as well. These low recovery rates may very well lead to a false ER.

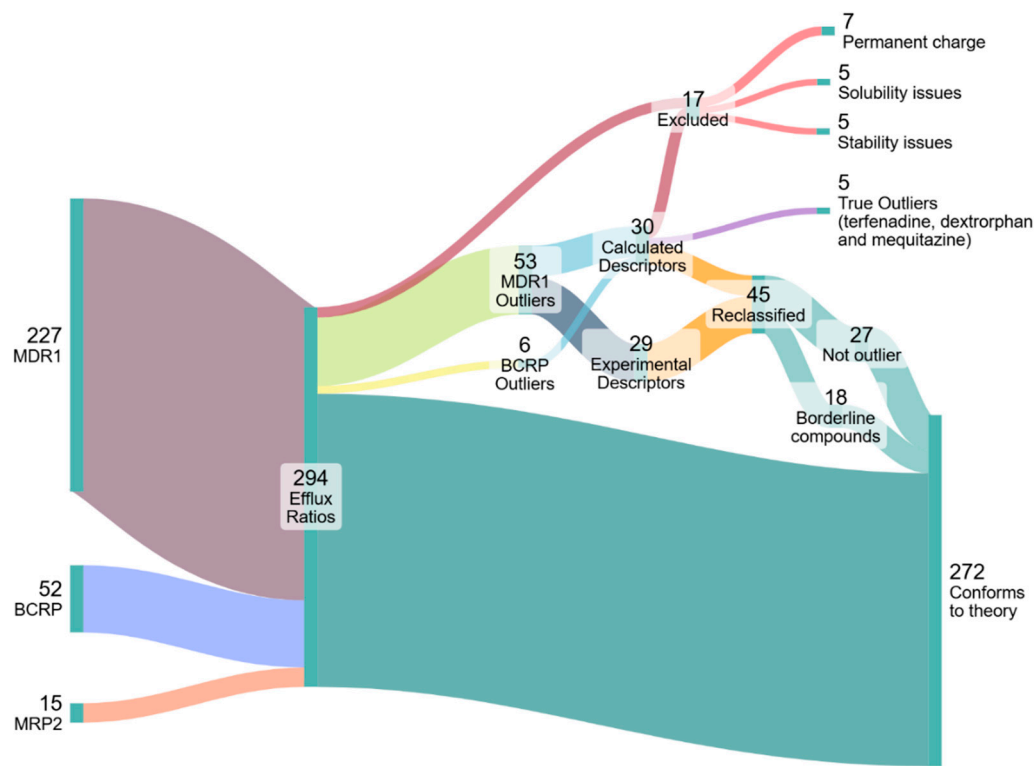


Figure 4. Diagram illustrating the categorization and analysis of 294 efflux ratios (136 distinct compounds) derived from MDR1, BCRP, and MRP2 transporter datasets. Certain chemicals were excluded for having a permanent charge, or for exhibiting solubility stability issues. Outliers were identified and investigated with MDCK or HDM-PAMPA assays, or by alternative methods. As is evident, the vast majority of outliers were reclassified and found to conform to the energy limitation theory, as 90% of the data supports the existence of a membrane permeability cut-off for compounds exhibiting significant efflux.

4.4. Concentration-Dependent Investigation of Borderline Compounds

Figure 5 shows the results of the concentration-dependence assays for a borderline compound (amprenavir) compared to a low P_m compound (acebutolol). The top panels show ER values as a function of applied assay concentration. The bottom panels show the $J_{pgp,active}$ values ($\mu\text{mol}/\text{cm}^2/\text{s}$) calculated from the $P_{app,A \rightarrow B}$ values at each concentration (Section 3.2.4). Similar graphs for all compounds tested can be found in the Supplementary Materials S1 (Sections S6, S10–S12), along with tabulated P_{app} , recovery and ER values at each concentration.

For the low P_m compound acebutolol, P-gp has not reached saturation, and there is no change in ER values even at very high concentrations. In contrast, for the borderline compound amprenavir, the decline in ER values is attributed to classic saturation effects of the P-gp transporter. This supports our theory that there is concentration-dependent saturation of active transport for compounds near the maximal flux limit. The decline in ER can be attributed to classic saturation effects of the P-gp transporter. At lower concentrations of the compound, the P-gp transporter is not saturated, leading to high transport rates and consequently high ER values. At higher compound concentrations, the transporter has likely reached saturation, and active transport does not further increase with concentration, meaning $P_{pgp,app}^{active}$ decreases. Therefore, passive permeation (permeability \times concentration) becomes more dominant as it increases proportionally to concentration, since P_m is expected to remain constant.

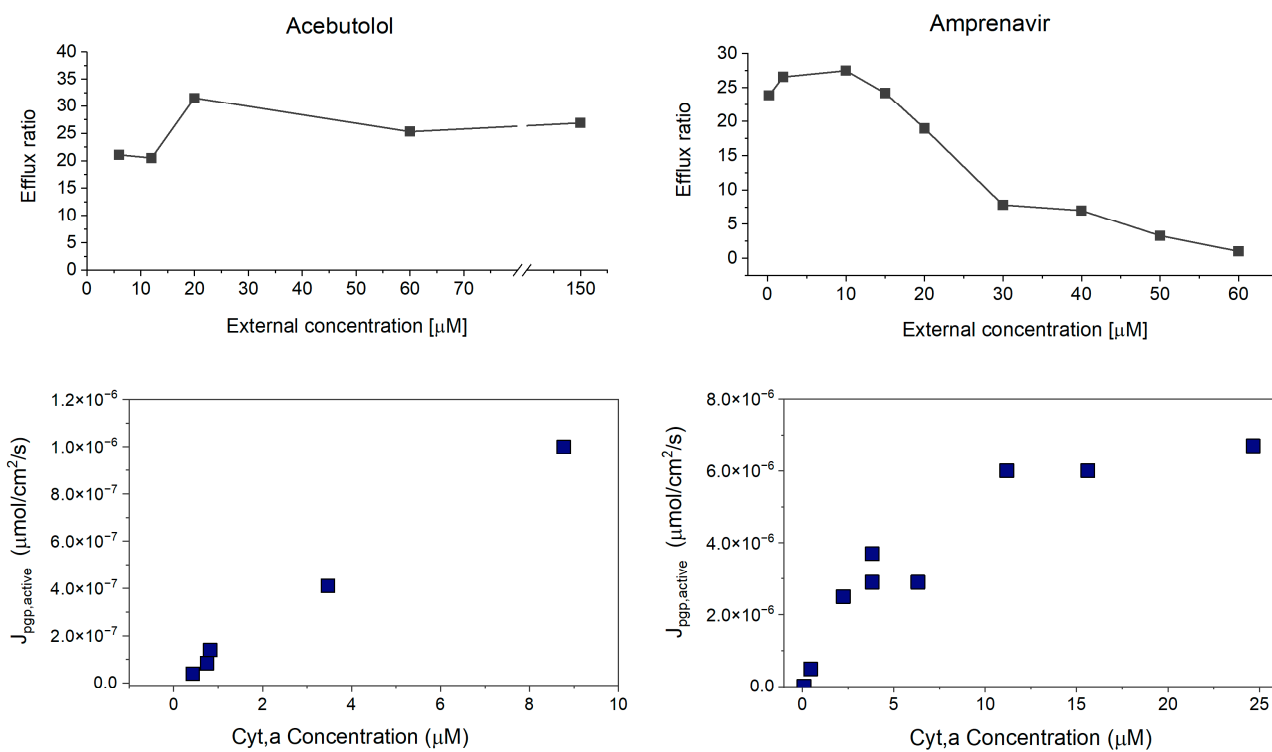


Figure 5. ER vs. external concentration for the borderline compound amprenavir (top), compared to the low P_m compound acebutolol (bottom). For borderline compounds, the ER decreases with increasing concentration. For the low P_m compound, the ER stays constant even at high external concentrations.

The observed saturation effects coinciding with the energy plateau are unlikely to be coincidental. Both phenomena result in the same outcome: no further increase in transporter activity with increasing concentration beyond a certain maximum flux value. As such, the energy limit imposed by physical principles is enforced by the cell through the mechanism of saturation. While transporter saturation and its effect on transporter-facilitated efflux have been described previously [82–84], this research is, to our knowledge, the first to associate it with an energy threshold. It is important to note that this does not imply that every observed saturation effect is caused by an energetic limitation; rather, a saturation effect is always observed before the energetic limit is reached, which is plausible from an evolutionary perspective, as it avoids the energy depletion of the cell. It is unclear how exactly the saturation effect would be linked to the energy limit. One hypothesis is that ATP binding kinetics may become rate-limiting at high active transport rates; however, this potential relationship is beyond the scope of the present study.

Tachibana et al. [85] previously applied a sophisticated model to extract $J_{pgp,active,max}$ (referred to as V_{max} in their work) from concentration-dependent measurements reported by Shirasaka et al. [86] for verapamil, vinblastine, and quinidine. Their model accounted for passive permeation into and out of the cell on both the apical and basolateral sides of the membrane, as well as unidirectional P-gp transport. While our model for obtaining the K_m value differs from theirs, both approaches use the intracellular K_m parameter relevant for transporter saturation rather than the extracellular one. The main difference between their approach and ours is that we also included paracellular transport and ABL resistance. It should be emphasized that ABL resistance cannot simply be lumped together with passive permeability; only passive permeability runs in parallel with active transport, whereas the ABL does not. Moreover, paracellular transport can strongly influence P_{app} , since P_{app} will not fall below P_{para} , even when P_{trans} is negligibly low because of active efflux.

Unfortunately, re-analyzing their published data with our model did not yield reliable results, see Supplementary Materials S1 (Section S7). A fourth compound, digoxin, was included in the study by Shirasaka et al. [86]. It showed no signs of saturation across the tested concentration range (up to 26 μ M). With a P_0 of 4.14 [32], corresponding to a $\log P_m \times C_{ext}$ of -2.72 , this completely neutral compound lies well below our permeability threshold—fully consistent with our model. Finally, the V_{max} of 5.7×10^{-6} μ mol/cm²/s for quinidine, obtained by Heikkinen et al. [84] using a five-compartment model that accounted for ABL effects, is in good agreement with our own $J_{pgp,active,max}$ of 9.7×10^{-6} μ mol/cm²/s (for $SA = 1$) derived from our quinidine experiments.

Therefore, it is worth reiterating that the conditions under which the experiments are conducted are critical for obtaining meaningful results in MDCK efflux assays. We have previously demonstrated that ER values can change based on the pH [21], which means that pH can play a role in the misclassification of compounds. In this work we show that using concentrations that are too high can also result in the erroneous conclusion that compounds are not P-gp substrates.

4.5. Empirical Determination of the Energy Limit

Four out of the six compounds suspected to be borderline compounds (for which concentration-dependent assays were performed) exhibited the expected plateau when the transport of these compounds started reaching the maximal $J_{pgp,active}$. Due to the observation of saturation effects with these compounds which evidently reached the maximal flux plateau, Michaelis–Menten fits were conducted as described in Section 3.2.5, the results of which are depicted in Figure 6. The final $J_{pgp,active,max}$ value was determined from the average of the individual maximum flux values determined for the four compounds depicted in Figure 6. Analogous fits for the same compounds using the other apical membrane surface area factors of 1 and 24 as well as the resultant mean $J_{pgp,active}$ values in these cases can be found in the Supplementary Materials S1 (Sections S13–S15). The mean ($N = 4$) $J_{pgp,active}$ determined for the case considered as most plausible (apical membrane surface area factor of 7.5) was determined to be 1.6×10^{-4} μ mol/cm²/s (range: 8.7×10^{-6} to 4.4×10^{-4} μ mol/cm²/s). This value is quite similar to a rough estimate of 7.4×10^{-5} μ mol/cm²/s obtained from mechanistic energy constraint considerations outlined in S1 (Section S2).

Since the maximal flux value is based on cellular energy constraints, we expect that all borderline compounds should plateau at the same maximal $J_{pgp,active}$. As is evident from Figure 6, this is not quite the case. This is easily explained when one considers the influence of P_0 values in determining $J_{pgp,active}$. P_0 values always come with some threshold of error, and the source of the P_0 is the biggest determining factor of the level of error. Quinidine has a very reliable experimental P_0 value determined from MDCK assays, whereas amprenavir and eletriptan both also have experimental (PAMPA-SDM) P_0 values. The results for loperamide, in contrast, are considered less precise because of uncertainty in predicted P_0 values. The P_0 for loperamide could not be determined via MDCK or PAMPA assays and, as such, is based on a SDM prediction. Although SDM predictions based on experimental descriptors can be fairly accurate, experimental P_0 are more reliable. The uncertainty in the P_0 prediction for loperamide consequently leads to greater uncertainty in its fitted $J_{pgp,active,max}$ values. Though experimental P_0 values are generally reliable, they are still subject to error. The experimental P_0 values for quinidine, amprenavir and eletriptan could still result in an estimation that is off by one order of magnitude. Thus, the maximal $J_{pgp,active}$ determined from these fits are fairly consistent within the inextricable error that comes with P_0 values.

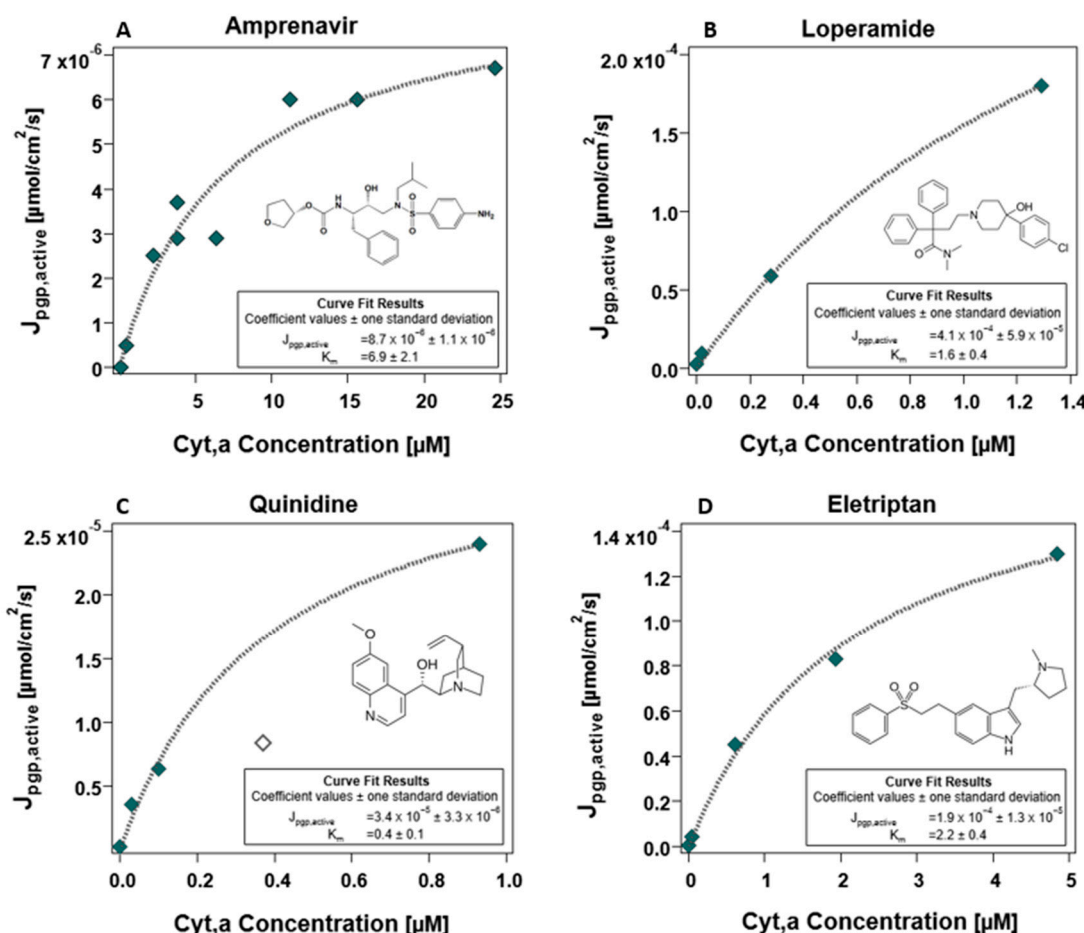


Figure 6. Non-linear Michaelis–Menten fits for borderline compounds exhibiting the maximal flux ($J_{\text{pgp,active}}$) plateau, for (A) amprenavir, (B) loperamide, (C) quinidine and (D) eletriptan. Markers represent the concentration-dependent calculated $J_{\text{pgp,active}}$ values, which are derived from fitted P-gp activity values obtained from MDCK assays. For the compound quinidine (C), the unfilled marker was not included in the fit.

This maximum $J_{\text{pgp,active}}$ of $1.6 \times 10^{-4} \mu\text{mol}/\text{cm}^2/\text{s}$ obtained from the Michaelis–Menten fits for four borderline compounds represents the energy threshold for efflux transport determined for the MDCKII-MDR1 cells utilized in this work. Essentially: it is unlikely that highly membrane-permeable compounds with greater flux demands for its effective efflux would be affected by any efflux transporter. As previously mentioned, compounds that are located within the borderline window of membrane permeability may exhibit efflux, depending on their concentration.

4.6. Linking a Passive Membrane Permeability Threshold to the Energy Limit

While the $J_{\text{pgp,active}}$ value is interesting, it must be linked with a more accessible metric such as membrane permeability to be useful in practice. As described earlier, for high ER $J_{\text{pgp,active}} \approx J_{\text{passive,in}}$, meaning almost all compound passively diffusing into the cell is actively transported out again. If the membrane poses the main resistance, $J_{\text{passive,in}}$ corresponds to $P_m \times C_{\text{ext}}$. However, this assumption is not valid for low ER values, or if other transport resistances are dominant. We thus used our model to calculate the maximum P_m that would lead to a specific ER assuming a maximal $J_{\text{pgp,active}}$ of $1.6 \times 10^{-4} \mu\text{mol}/\text{cm}^2/\text{s}$ as described in Section 3.2.5, see also Supplementary Materials S1 (Section S16).

As is evident from Figure 7, the $P_m \times C_{\text{ext}}$ threshold stays constant across all ER values, except in the lower ranges. To appreciate why this is, it must be considered that at low ER

values where P-gp activity is diminished, the passive backflow of the compound from the cytosol is significant. This does not apply for compounds exhibiting high ER values where P-gp is more active, see Supplementary Materials S1 (Section S17). However, this affects only a small fraction of the significant efflux ratios in our database, specifically those that just exceed the significance threshold. Therefore, the plateau remains the most interesting value. However, this sharp increase in the $P_m \times C_{ext}$ limit for low ER values might explain the few remaining outliers that did indeed show low ER values (2.6–2.8). Especially when one considers that low recovery may also have resulted in an overestimation of ER.

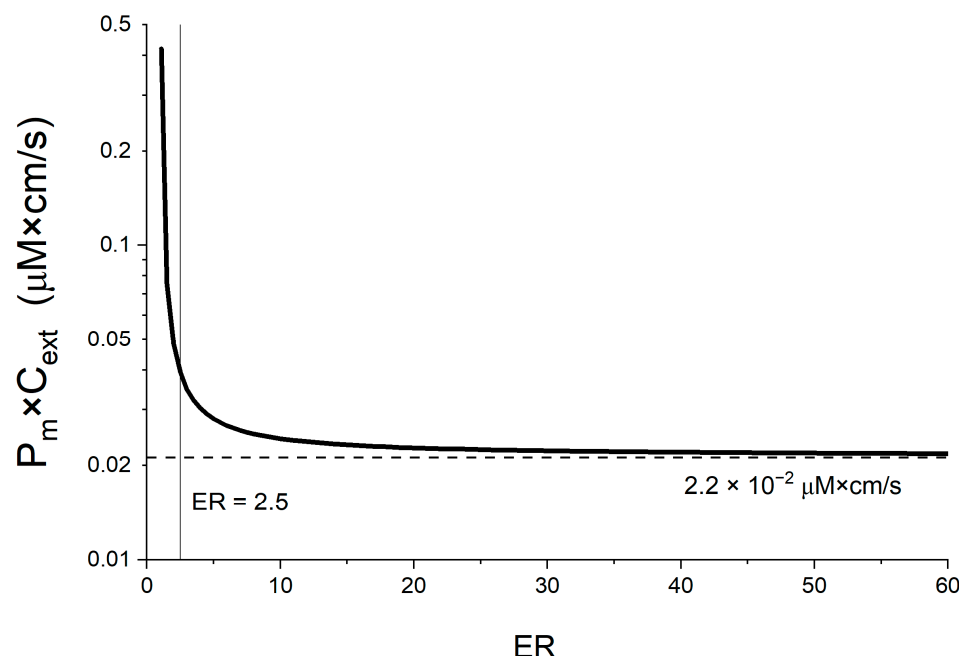


Figure 7. The $P_m \times C_{ext}$ threshold associated with the maximal $J_{pgp,active}$ value of $1.6 \times 10^{-4} \mu\text{mol}/\text{cm}^2/\text{s}$ as a function of ER values. The threshold lies at a value of $\log(P_m \times C_{ext}) = -1.7$.

4.7. Sensitivity Analysis of P_m Threshold

Although the energy threshold should remain static among different compounds and concentrations, the conversion of $J_{pgp,active}$ into a P_m value is influenced by several factors. Firstly, the apical membrane surface area factor SA is expected to be quite consequential, as this directly affects the maximal $J_{pgp,active}$ value (see Figures S11–S13). Fortunately, SA does not affect the extracted P_m threshold if we consider the maximal $J_{pgp,active}$ that corresponds with the respective SA. For example, if the SA is increased by 3.2 (as is the case with 7.5 vs. 24), the extracted $J_{pgp,active}$ is also increased by a factor of 3.2, but the extracted $P_m \times C_{ext}$ threshold is not affected (see Figure S10). Regardless of which surface area is assumed, saturation always occurs for the same set of permeable compounds at the same concentration, so the limiting value of permeability \times concentration remains constant. The empirical determination of the $P_m \times C_{ext}$ threshold specific to our cells is thus not affected by the uncertainty of the SA factor. However, if a fixed maximal $J_{pgp,active}$ is used to extract P_m , the resulting values will scale directly with SA (see Figure S11), which is of relevance if the threshold is determined by theoretical deliberations on the energy limit, and not empirically. This becomes critical when the energy limit is determined independently (e.g., from ATP-turnover rates, see Supplementary Materials S1 (Section S2)) because SA variability would then introduce a major source of uncertainty.

Secondly, as stated in the preceding section, the maximal $J_{pgp,active}$ presented in this work was determined specifically for MDCK-MDR1 cells. The maximum flux value can vary among different cell types. Since the energy needs of MDCK cells are higher than that

of other, less active cells (see Supplementary Materials S1 (Section S2)), they likely have a higher energy limit than the average cell. Therefore, it is essential to note that variations will exist between different cell types. Cells with increased energy demands/production are likely to exhibit a higher maximum flux value. For example, in cancer cells an upregulation of mitochondrial respiration has been reported [87], which would also suggest an increased $J_{pgp,active,max}$. The observation that inhibition of the electron transport chain restored the cells' drug sensitivity [87] is fully consistent with our assumption of an energy limitation.

The energy limit of the cells, and thus their maximal $J_{pgp,active}$, was found to be directly proportional to the corresponding P_m threshold. The observed variability in maximal $J_{pgp,active}$ (range 8.7×10^{-6} to $4.4 \times 10^{-4} \mu\text{mol}/\text{cm}^2/\text{s}$) thus directly translates to a range of the $\log(P_m \times C_{ext})$ threshold of -2.94 to -1.23 . An increase in maximum flux shifts the $\log P_m$ threshold higher by the same factor. Therefore, it is important to reiterate that the P_m threshold provided here is not a universal figure, as it was established for the MDCK-MDR1 cells available to us. Consequently, the same P_m cut-off cannot be applied uniformly across all cell types. For instance, cells in the blood–brain barrier (BBB) exhibit greater activity compared to Caco-2 cells because they have high expression of various efflux transporters to tightly regulate brain access [88]. Thus, if BBB cells demonstrate a greater maximum flux value, it stands to reason that this would enable the effective efflux of compounds with increased passive membrane permeability. The higher density of mitochondria in the blood–brain barrier [89] may result in a higher energetic limit (and thus higher $P_m \times C_{ext}$ threshold). This—together with the typically lower compound concentrations in blood compared to the intestine—may explain why certain compounds exhibit high bioavailability but low brain uptake, if they are not actively effluxed in the gut but are in the brain (even though passive membrane permeability is similar in the gut and the brain [90]).

Finally, the importance of concentration for the P_m threshold was very apparent. As expected it was found that the P_m threshold is indirectly proportional to the concentration, since their product determines the passive diffusive flux rate through the membrane that counteracts active transport. As the concentration of the compound decreases, the threshold rises (and the opposite is true for increasing concentrations). This is why the metric proposed for the threshold is not simply P_m , but rather the P_m -concentration product, $P_m \times C_{ext}$ ($\mu\text{M cm/s}$).

The effect of paracellular transport, compound charge, as well as basolateral uptake on the $P_m \times C_{ext}$ threshold was also evaluated, but was found to be inconsequential (Figures S12–S14). Thus, the final $\log(P_m \times C_{ext})$ threshold for our MDCK-MDR1 cell system—determined empirically with borderline compounds—was found to lie at -1.7 . This is slightly higher than the threshold considered initially for the identification of outliers, and as such did not result in the re-identification of more outliers not previously considered.

4.8. Re-Evaluation of Literature Data

294 significant ER values from MDCK assays were gathered from 46 different sources in the literature. Based on the spread of the starting experimental data, it was initially hypothesized that for MDCK cells, compounds with a $P_m \times C_{ext}$ value exceeding $1 \times 10^{-2} \text{ cm/s}$ would be too membrane-permeable for the cell to maintain effective efflux against their high rates of passive diffusion. Two-thirds of the data did not contradict this hypothesis from the outset. In other words, these compounds were confirmed efflux substrates with a $P_m \times C_{ext}$ lower than $1 \times 10^{-2} \text{ cm/s}$. Figure 8 shows the distribution of the data of all three transporters after re-evaluation of the outliers, along with the final $P_m \times C_{ext}$ threshold line of $2.2 \times 10^{-2} \text{ cm/s}$ (and borderline area) that was determined empirically in this study.

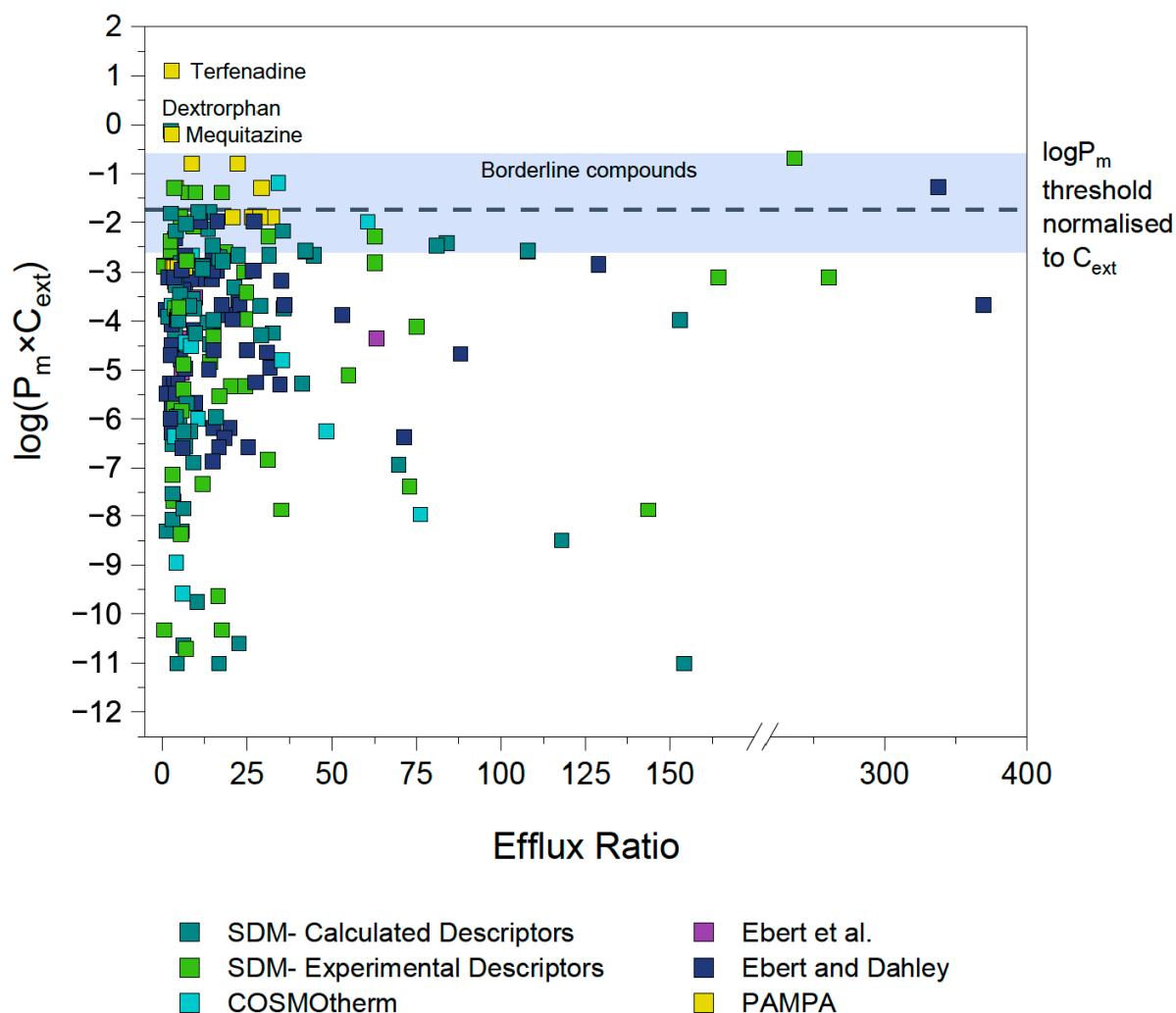


Figure 8. $\log(P_m \times C_{ext})$ vs. ER of re-evaluated data from all transporter (P-gp, BCRP and MRP2) datasets. The $\log(P_m \times C_{ext})$ threshold for the MDCKII-MDR1 cells was determined to be -1.7 . With the exception of the three indicated outlier compounds, no compounds with $P_m \times C_{ext}$ above $2.2 \times 10^{-2} \text{ cm/s} \times \mu\text{M}$ showed significant efflux. The efflux of borderline compounds is highly dependent on concentration. Experimental P_m values sourced from Ebert et al. [32] and Ebert and Dahley [26].

The depicted $P_m \times C_{ext}$ threshold is based on the $J_{p\text{gp,active,max}}$ of $1.6 \times 10^{-4} \mu\text{mol/cm}^2/\text{s}$ determined for our MDCK-MDR1 cells. Due to normalization of the threshold P_m to external concentration, it is independent of assay concentration used.

It is remarkable that among all compounds analyzed here and documented in the literature as being substrates of one of the three primary efflux transporters associated with MDR, all have $P_m \times C_{ext}$ values either below the threshold, or they fall in the borderline window and exhibit only concentration-dependent efflux. This supports the theory that there is indeed a P_m limit for active efflux—and due to it being based on the fundamental principle of cellular energy constraints, that it is universal for three different transporters. Ultimately, there are only three unconvincing, low ER compounds which have a $P_m \times C_{ext}$ value exceeding the threshold and its corresponding borderline window. This is notable as there is no shortage of pharmaceutical compounds with $\log(P_m \times C_{ext})$ values above the threshold. As described in Section 3.2.1, 123 compounds with non-significant ER values were also evaluated. Figure 9 depicts the $P_m \times C_{ext}$ values for these compounds with ER values less than 2.5 in red, and as is evident about 60% of them fall above the threshold. Compounds below the threshold may potentially be affected by efflux transport, and

in vitro transwell assays for these compounds are warranted. However, compounds above the threshold are not expected to be affected by efflux transporters, and assays to check for an ER value would be unnecessary.

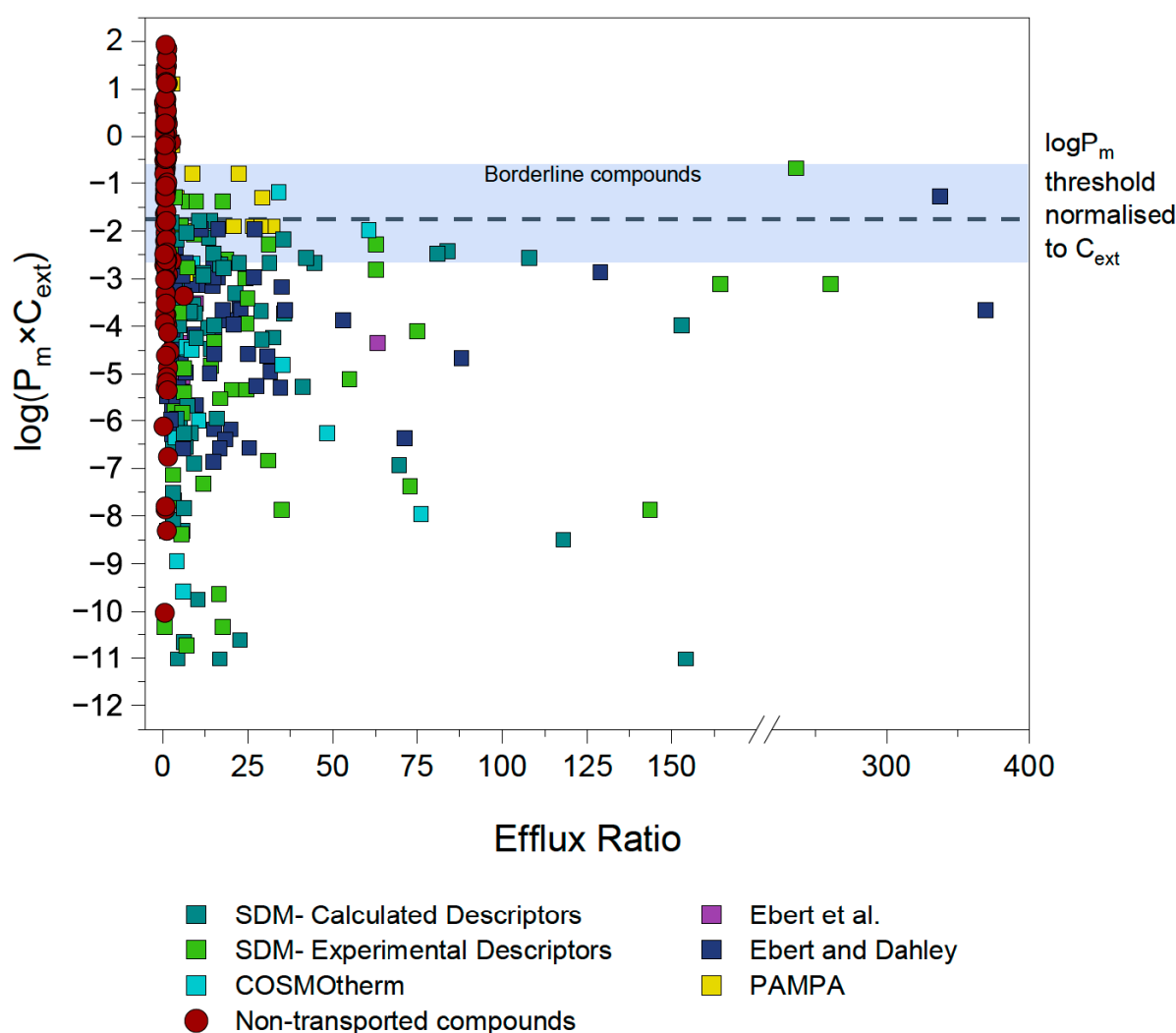


Figure 9. $\log(P_m \times C_{ext})$ vs. ER of re-evaluated data from all transporter (P-gp, BCRP and MRP2) datasets, along with non-transported compounds in red. Experimental P_m values sourced from Ebert et al. [32] and Ebert and Dahley [26].

Our results align with the Biopharmaceutics Drug Disposition Classification System (BDDCS), which categorizes drugs into four classes according to solubility and intestinal permeability. According to Benet et al. [91], efflux transport should be considered for Class II compounds (low solubility, high passive permeability), whereas membrane transporters—both uptake and efflux—play a critical role for Class III (high solubility, low permeability) and Class IV (low solubility, low permeability) drugs. In contrast, for Class I drugs (high solubility, high permeability), active transport is generally not relevant. This is fully consistent with our defined $P_m \times C_{ext}$ threshold, since we would not anticipate active transport under conditions of high permeability combined with high concentrations.

5. Conclusions

In this study, we propose an energy limit for active efflux, which can be translated into a membrane permeability threshold to simplify identification of compounds that may exhibit significant efflux. We collected nearly 300 ER values from the MDCK assays of three

transporters (P-gp, BCRP and MRP2) from the existing literature to investigate this premise. After establishing a preliminary threshold, a systematic analysis of outliers (compounds with ER values > 2.5 and $\log(P_m \times C_{ext})$ values > -2) led to the reclassification of most outliers as conformers. Concentration-dependent transwell assays for borderline compounds enabled the more precise identification of the maximal flux value ($J_{pgp,active,max}$) of $1.6 \times 10^{-4} \mu\text{mol}/\text{cm}^2/\text{s}$ for our MDCK-MDR1 cell systems. It was found that the energy limit seems to be enforced by the cell through the mechanism of saturation. The maximal $J_{pgp,active}$ was then translated into a more accessible threshold P_m value. The threshold P_m was normalized to external concentration for a concentration-independent $P_m \times C_{ext}$ threshold. This $P_m \times C_{ext}$ threshold falls within the mid-range of typical hydrophobicity/lipophilicity values for most chemicals of interest, making it relevant across a broad spectrum of compounds.

Our results confirm that passive membrane permeability ($P_m \times C_{ext}$) can be used as a filtering metric to determine whether the pharmacokinetics of pharmaceutical compounds can be affected by efflux. However, accurate P_m values are critical for this determination. The model should be applicable to other cell lines or tissues, as the underlying principle—that active transport must counteract passive permeation and that energy consumption is inherently limited—is universal to all cells. However, the specific threshold will need to be determined for each cell type, as different cells have different energy budgets. One approach could be to estimate the threshold directly from the energy budget of the considered cell types, although parameters such as surface area, stoichiometry, and ATP turnover introduce additional uncertainties, and the practicability of this approach will need to be evaluated in future studies. A more direct and robust alternative is to determine the precise $P_m \times C_{ext}$ threshold experimentally using borderline compounds on the cell line of interest, as we did in this study, which minimizes uncertainties related the above-mentioned factors.

The new approach would reduce the need for time- and resource-intensive transport assays for compounds above the threshold and would assist with the design of in vitro experiments that avoid saturation effects, thereby minimizing false negatives. In addition, it can aid rational lead optimization by allowing drugs of interest to be engineered for desired transporter interactions through adjustments in passive membrane permeability. A key practical limitation—shared with in vitro assays—is that the freely dissolved concentration (e.g., in the gut for oral absorption studies or in blood for blood–brain barrier studies) must be known, as it directly influences the threshold. We recognize that in physiological scenarios, multiple transporters may act synergistically, cellular energy may fluctuate under pathological conditions, and genetic polymorphisms can alter transporter activity. Our model assumes constant stoichiometry for ATP-dependent efflux transporters; under this assumption, synergistic transport by different transporter types does not change the total energy required to transport a given number of molecules. Nevertheless, variations in stoichiometry, energy limitation, or polymorphisms could alter the effective threshold, representing important limitations and avenues for future investigation. In the future, our quantitative framework may provide a basis for refining strategies to prevent active efflux through induced intracellular ATP depletion [92–95], although such applications remain to be explored. Overall, this novel mechanistic approach, grounded in cellular energy constraints, offers a promising way to predict when active efflux is unlikely solely from the chemical structure.

Supplementary Materials: The following supporting information can be downloaded at: <https://www.mdpi.com/article/10.3390/pharmaceutics1711455/s1>. Figure S1: Physiological and cellular approaches towards calculating theoretical maximal flux values; Figure S2: Apparent permeability and efflux ratios as a function of concentration for the compounds acebutolol, amprenavir, loperamide, eletriptan, nelfinavir, prazosin and quinidine; Figure S3: Three-compartment model simulations

of the concentration over time in the different compartments in the $B \rightarrow A$ direction; Figure S4: P-gp facilitated flux fit values versus concentration for seven compounds with $S = 1$; Figure S5: P-gp facilitated flux fit values versus concentration for seven compounds with $S = 7.5$; Figure S6: P-gp facilitated flux fit values versus concentration for seven compounds with $S = 24$; Figure S7: Michaelis-Menten fits of $J_{pgp,active}$ values for apical surface membrane factor = 1 and mean maximal $J_{pgp,active}$ values; Figure S8: Michaelis-Menten fits of $J_{pgp,active}$ values for apical surface membrane factor = 7.5 and mean maximal $J_{pgp,active}$ values; Figure S9: Michaelis-Menten fits of $J_{pgp,active}$ values for apical surface membrane factor = 24 and mean maximal $J_{pgp,active}$ values; Figure S10: The $P_m \times C_{ext}$ threshold as a function of ER values extracted from our experiments assuming different SA, as indicated; Figure S11: The $P_m \times C_{ext}$ threshold associated with a fixed maximal $J_{pgp,active}$ value of $1.6 \times 10^{-4} \mu\text{mol}/\text{cm}^2/\text{s}$ as a function of ER values for different SA; Figure S12: The $P_m \times C_{ext}$ threshold associated with a fixed maximal $J_{pgp,active}$ value of $1.6 \times 10^{-4} \mu\text{mol}/\text{cm}^2/\text{s}$ as a function of ER values based on magnitude of basolateral uptake transporter activity; Figure S13: The $P_m \times C_{ext}$ threshold associated with a fixed maximal $J_{pgp,active}$ value of $1.6 \times 10^{-4} \mu\text{mol}/\text{cm}^2/\text{s}$ as a function of ER values based on the whether the compound is charged or neutral; Figure S14: The $P_m \times C_{ext}$ threshold associated with a fixed maximal $J_{pgp,active}$ value of $1.6 \times 10^{-4} \mu\text{mol}/\text{cm}^2/\text{s}$ as a function of ER values based on the magnitude of paracellular transport; Table S1: Pgp dataset: Chemical properties and P_m values; Table S2 BCRP dataset: Chemical properties and calculated P_m values; Table S3 MRP2 dataset: Chemical properties and calculated P_m value; Table S4 Concentration-corrected P_m values for all transporters; Table S5 P_m values calculated from PAMPA $K_{hex/w}$ values; Table S6 Outliers analysis; Table S7 Compounds with insignificant ER values: Chemical properties and P_m values; Table S8 Concentration-corrected P_m values for compounds with insignificant ER values. References [96–115] are only cited in the Supplementary Materials.

Author Contributions: Conceptualization, K.-U.G. and A.E.; Methodology, S.K. and A.E.; Formal analysis, S.K. and A.E.; Writing—original draft, S.K.; Writing—Review and Editing, K.-U.G. and A.E.; Visualization, S.K.; Supervision, K.-U.G. All authors have read and agreed to the published version of the manuscript.

Funding: This research did not receive any specific grant from funding agencies in the public, commercial, or not-for-profit sectors.

Institutional Review Board Statement: Not applicable.

Informed Consent Statement: Not applicable.

Data Availability Statement: The datasets used and/or analyzed during the current study are available from the corresponding author upon request.

Acknowledgments: This work is based on a Ph.D. thesis completed at Martin-Luther-Universität Halle-Wittenberg in Halle, Germany in 2025. Full thesis metadata: Title—‘Active Transport Across Biological Membranes: Quantification and Limits’, Author—‘Soné Kotze’, University—‘Martin-Luther-Universität Halle-Wittenberg’, Location—‘Halle’, Country—‘Germany’, Date—‘2025’. This work was previously published as a preprint on Preprints.org with DOI 10.20944/preprints202510.0746.v1.

Conflicts of Interest: The authors declare that they have no known competing financial interests or personal relationships that could have appeared to influence the work reported in this paper.

References

1. Galetin, A.; Brouwer, K.L.R.; Tweedie, D.; Yoshida, K.; Sjöstedt, N.; Aleksunes, L.; Chu, X.; Evers, R.; Hafey, M.J.; Lai, Y.; et al. Membrane transporters in drug development and as determinants of precision medicine. *Nat. Rev. Drug Discov.* **2024**, *23*, 255–280. [\[CrossRef\]](#)
2. Juvale, A.; Abdul Hamid, A.A.; Abd Halim, K.B.; Che, H. *P-glycoprotein: New Insights into Structure, Physiological Function, Regulation and Alterations in Disease*, in *Heliyon*; Elsevier Ltd.: Amsterdam, The Netherlands, 2022.
3. Sharom, F.J. ABC multidrug transporters: Structure, function and role in chemoresistance. *Pharmacogenomics* **2007**, *9*, 105–127. [\[CrossRef\]](#)

4. Duan, C.; Yu, M.; Xu, J.; Li, B.-Y.; Zhao, Y.; Kankala, R.K. Overcoming Cancer Multi-drug Resistance (MDR): Reasons, mechanisms, nanotherapeutic solutions, and challenges. *Biomed. Pharmacother.* **2023**, *162*, 114643. [\[CrossRef\]](#)
5. Tian, Y.; Lei, Y.; Wang, Y.; Lai, J.; Wang, J.; Xia, F. Mechanism of multidrug resistance to chemotherapy mediated by P-glycoprotein (Review). *Int. J. Oncol.* **2023**, *63*, 119. [\[CrossRef\]](#)
6. Demel, M.A.; Krämer, O.; Ettmayer, P.; Haaksma, E.E.J.; Ecker, G.F. Predicting ligand interactions with ABC transporters in ADME. *Chem. Biodivers.* **2009**, *6*, 1960–1969. [\[CrossRef\]](#)
7. Waghray, D.; Zhang, Q. Inhibit or Evade Multidrug Resistance P-Glycoprotein in Cancer Treatment. *J. Med. Chem.* **2018**, *61*, 5108–5121. [\[CrossRef\]](#) [\[PubMed\]](#)
8. Li, D.; Chen, L.; Li, Y.; Tian, S.; Sun, H.; Hou, T. ADMET evaluation in drug discovery. 13. Development of in silico prediction models for p-glycoprotein substrates. *Mol. Pharm.* **2014**, *11*, 716–726. [\[CrossRef\]](#) [\[PubMed\]](#)
9. Wang, Z.; Chen, Y.; Liang, H.; Bender, A.; Glen, R.C.; Yan, A. P-glycoprotein substrate models using support vector machines based on a comprehensive data set. *J. Chem. Inf. Model.* **2011**, *51*, 1447–1456. [\[CrossRef\]](#)
10. Chen, L.; Li, Y.; Yu, H.; Zhang, L.; Hou, T. Computational models for predicting substrates or inhibitors of P-glycoprotein. *Drug Discov. Today* **2012**, *17*, 343–351. [\[CrossRef\]](#)
11. Adachi, A.; Yamashita, T.; Kanaya, S.; Kosugi, Y. Ensemble Machine Learning Approaches Based on Molecular Descriptors and Graph Convolutional Networks for Predicting the Efflux Activities of MDR1 and BCRP Transporters. *AAPS J.* **2023**, *25*, 88. [\[CrossRef\]](#)
12. Esposito, C.; Wang, S.; Lange, U.E.W.; Oellien, F.; Riniker, S. Combining Machine Learning and Molecular Dynamics to Predict P-Glycoprotein Substrates. *J. Chem. Inf. Model.* **2020**, *60*, 4730–4749. [\[CrossRef\]](#) [\[PubMed\]](#)
13. Seelig, A. A general pattern for substrate recognition by P-glycoprotein. *Eur. J. Biochem.* **1998**, *251*, 252–261. [\[CrossRef\]](#) [\[PubMed\]](#)
14. Didzaiapetris, R.; Japertas, P.; Avdeef, A.; Petruskas, A. Classification analysis of P-glycoprotein substrate specificity. *J. Drug Target.* **2003**, *11*, 391–406. [\[PubMed\]](#)
15. Gombar, V.K.; Polli, J.W.; Humphreys, J.E.; Wring, S.A.; Serabjit-Singh, C.S. Predicting P-Glycoprotein Substrates by a Quantitative Structure-Activity Relationship Model. *J. Pharm. Sci.* **2003**, *4*, 957–968. [\[CrossRef\]](#)
16. Konig, C.; Vellido, A. Understanding predictions of drug profiles using explainable machine learning models. *BioData Min.* **2024**, *17*, 25. [\[CrossRef\]](#)
17. Zhang, Y.; Wu, J.; Kang, Y.; Hou, T. A multimodal contrastive learning framework for predicting P-glycoprotein substrates and inhibitors. *J. Pharm. Anal.* **2025**, *15*, 101313. [\[CrossRef\]](#)
18. Karami, T.K.; Hailu, S.; Feng, S.; Graham, R.; Gukasyan, H.J. Eyes on Lipinski’s Rule of Five: A New “Rule of Thumb” for Physicochemical Design Space of Ophthalmic Drugs. *J. Ocul. Pharmacol. Ther.* **2022**, *38*, 43–55. [\[CrossRef\]](#)
19. Wu, K.; Kwon, S.H.; Zhou, X.; Fuller, C.; Wang, X.; Vadgama, J.; Wu, Y. Overcoming Challenges in Small-Molecule Drug Bioavailability: A Review of Key Factors and Approaches. *Int. J. Mol. Sci.* **2024**, *25*, 13121. [\[CrossRef\]](#)
20. Dahley, C.; Böckmann, T.; Ebert, A.; Goss, K.U. Predicting the intrinsic membrane permeability of Caco-2/MDCK cells by the solubility-diffusion model. *Eur. J. Pharm. Sci.* **2024**, *195*, 106720. [\[CrossRef\]](#)
21. Kotze, S.; Goss, K.-U.; Ebert, A. The pH-dependence of efflux ratios determined with bidirectional transport assays across cellular monolayers. *Int. J. Pharm. X* **2024**, *8*, 100269. [\[CrossRef\]](#)
22. Schulz, M.; Schmoldt, A. Therapeutic and toxic blood concentrations of more than 800 drugs and other xenobiotics. *Pharmazie* **2003**, *58*, 447–474.
23. Ebert, A.; Hanneschlaeger, C.; Goss, K.U.; Pohl, P. Passive Permeability of Planar Lipid Bilayers to Organic Anions. *Biophys. J.* **2018**, *115*, 1931–1941. [\[CrossRef\]](#)
24. Escher, B.I.; Abagyan, R.; Embry, M.; Klüver, N.; Redman, A.D.; Zarfl, C.; Parkerton, T.F. Recommendations for Improving Methods and Models for Aquatic Hazard Assessment of Ionizable Organic Chemicals. *Environ. Toxicol. Chem.* **2020**, *39*, 269–286. [\[CrossRef\]](#) [\[PubMed\]](#)
25. ACD Percepta, version 2020.1.2; Advanced Chemistry Development, Inc. (ACD/Labs): Toronto, ON, Canada, 2020. Available online: <https://www.acdlabs.com> (accessed on 1 September 2025).
26. Ebert, A.; Dahley, C. Can membrane permeability of zwitterionic compounds be predicted by the solubility-diffusion model? *Eur. J. Pharm. Sci.* **2024**, *199*, 106819. [\[CrossRef\]](#) [\[PubMed\]](#)
27. Palay, S.L.; Karlin, L.J. An Electron Microscopic Study of the Intestinal Villus II. The Pathway of Fat Absorption. *J. Biophys. Biochem. Cytol.* **1959**, *5*, 373–384. [\[CrossRef\]](#) [\[PubMed\]](#)
28. Butor, C.; Davoust, J. Apical to Basolateral Surface Area Ratio and Polarity of MDCK Cells Grown on Different Supports. *Exp. Cell Res.* **1992**, *203*, 115–127. [\[CrossRef\]](#)
29. Bittermann, K.; Goss, K.U. Predicting apparent passive permeability of Caco-2 and MDCK cell-monolayers: A mechanistic model. *PLoS ONE* **2017**, *12*, e0190319. [\[CrossRef\]](#)
30. UFZ-LSER. *UFZ-LSER Database v4.0*; Helmholtz Centre for Environmental Research-UFZ: Leipzig, Germany, 2025.
31. Eckert, F.; Klamt, A. Fast Solvent Screening via Quantum Chemistry: COSMO-RS Approach. *AIChE J.* **2002**, *48*, 369–385. [\[CrossRef\]](#)

32. Ebert, A.; Dahley, C.; Goss, K.U. Pitfalls in evaluating permeability experiments with Caco-2/MDCK cell monolayers. *Eur. J. Pharm. Sci.* **2024**, *194*, 106699. [\[CrossRef\]](#)

33. Dahley, C.; Goss, K.U.; Ebert, A. Predicting Caco-2/MDCK Intrinsic Membrane Permeability from HDM-PAMPA-Derived Hexadecane/Water Partition Coefficients. *Eur. J. Pharm. Sci.* **2025**, *214*, 107280. [\[CrossRef\]](#)

34. Wager, T.T.; Chandrasekaran, R.Y.; Hou, X.; Troutman, M.D.; Verhoest, P.R.; Villalobos, A.; Will, Y. Defining desirable central nervous system drug space through the alignment of molecular properties, in vitro ADME, and safety attributes. *ACS Chem. Neurosci.* **2010**, *1*, 420–434. [\[CrossRef\]](#)

35. Callegari, E.; Malhotra, B.; Bungay, P.J.; Webster, R.; Fenner, K.S.; Kempshall, S.; LaPerle, J.L.; Michel, M.C.; Kay, G.G. A comprehensive non-clinical evaluation of the CNS penetration potential of antimuscarinic agents for the treatment of overactive bladder. *Br. J. Clin. Pharmacol.* **2011**, *72*, 235–246. [\[CrossRef\]](#) [\[PubMed\]](#)

36. Feng, B.; Mills, J.B.; Davidson, R.E.; Mireles, R.J.; Janiszewski, J.S.; Troutman, M.D.; de Morais, S.M. In vitro P-glycoprotein assays to predict the in vivo interactions of P-glycoprotein with drugs in the central nervous system. *Drug Metab. Dispos.* **2008**, *36*, 268–275. [\[CrossRef\]](#) [\[PubMed\]](#)

37. Troutman, M.D.; Thakker, D.R. Novel Experimental Parameters to Quantify the Modulation of Absorptive and Secretory Transport of Compounds by P-Glycoprotein in Cell Culture Models of Intestinal Epithelium. *Pharm. Res.* **2003**, *20*, 1210–1224. [\[CrossRef\]](#)

38. Mahar Doan, K.M.; Humphreys, J.E.; Webster, L.O.; Wring, S.A.; Shampine, L.J.; Serabjit-Singh, C.J.; Adkison, K.K.; Polli, J.W. Passive permeability and P-glycoprotein-mediated efflux differentiate central nervous system (CNS) and non-CNS marketed drugs. *J. Pharmacol. Exp. Ther.* **2002**, *303*, 1029–1037. [\[CrossRef\]](#) [\[PubMed\]](#)

39. Polli, J.W.; Wring, S.A.; Humphreys, J.E.; Huang, L.; Morgan, J.B.; Webster, L.O.; Serabjit-Singh, C.S. Rational Use of in Vitro P-glycoprotein Assays in Drug Discovery. *J. Pharmacol. Exp. Ther.* **2001**, *299*, 620–628. [\[CrossRef\]](#)

40. Hellinger, É.; Veszelka, S.; Tóth, A.E.; Walter, F.; Kittel, Á.; Laura, M.; Tihanyi, K.; Háda, V.; Nakagawa, S.; Dinh, T.; et al. Comparison of brain capillary endothelial cell-based and epithelial (MDCK-MDR1, Caco-2, and VB-Caco-2) cell-based surrogate blood-brain barrier penetration models. *Eur. J. Pharm. Biopharm.* **2012**, *82*, 340–351. [\[CrossRef\]](#)

41. Wang, Q.; Rager, J.D.; Weinstein, K.; Kardos, P.S.; Dobson, G.L.; Li, J.; Hidalgo, I.J. Evaluation of the MDR-MDCK cell line as a permeability screen for the blood-brain barrier. *Int. J. Pharm.* **2005**, *288*, 349–359. [\[CrossRef\]](#)

42. Carrara, S.; Reali, V.; Misiano, P.; Dondio, G.; Bigogno, C. Evaluation of in vitro brain penetration: Optimized PAMPA and MDCKII-MDR1 assay comparison. *Int. J. Pharm.* **2007**, *345*, 125–133. [\[CrossRef\]](#)

43. Obradovic, T.; Dobson, G.G.; Shingaki, T.; Kungu, T.; Hidalgo, I.J. Assessment of the first and second generation antihistamines brain penetration and role of P-glycoprotein. *Pharm. Res.* **2007**, *24*, 318–327. [\[CrossRef\]](#)

44. Chen, C.; Hanson, E.; Watson, J.W.; Lee, J.S. P-Glycoprotein limits the brain penetration of nonsedating but not sedating H1-antagonists. *Drug Metab. Dispos.* **2003**, *31*, 312–318. [\[CrossRef\]](#)

45. Park, M.S.; Okochi, H.; Benet, L.Z. Is Ciprofloxacin a Substrate of P-glycoprotein? *Arch. Drug Inf.* **2011**, *4*, 1–9. [\[CrossRef\]](#) [\[PubMed\]](#)

46. Gertz, M.; Harrison, A.; Houston, J.B.; Galetin, A. Prediction of human intestinal first-pass metabolism of 25 CYP3A substrates from in vitro clearance and permeability data. *Drug Metab. Dispos.* **2010**, *38*, 1147–1158. [\[CrossRef\]](#) [\[PubMed\]](#)

47. Chang, C.; Bahadduri, P.M.; Polli, J.E.; Swaan, P.W.; Ekins, S. Rapid identification of P-glycoprotein substrates and inhibitors. *Drug Metab. Dispos.* **2006**, *34*, 1976–1984. [\[CrossRef\]](#) [\[PubMed\]](#)

48. Eriksson, U.G.; Dorani, H.; Karlsson, J.; Fritsch, H.; Hoffmann, K.-J.; Olsson, L.; Sarich, T.C.; Wall, U.; Schützer, K.-M. Influence of erythromycin on the pharmacokinetics of ximelagatran may involve inhibition of P-glycoprotein-mediated excretion. *Drug Metab. Dispos.* **2006**, *34*, 775–782. [\[CrossRef\]](#)

49. Taub, M.E.; Podila, L.; Ely, D.; Almeida, I. Functional assessment of multiple p-glycoprotein (P-gp) probe substrates: Influence of cell line and modulator concentration on P-gp activity. *Drug Metab. Dispos.* **2005**, *33*, 1679–1687. [\[CrossRef\]](#)

50. Huang, L.; Wang, Y.; Grimm, S. ATP-dependent transport of rosuvastatin in membrane vesicles expressing breast cancer resistance protein. *Drug Metab. Dispos.* **2006**, *34*, 738–742. [\[CrossRef\]](#)

51. De Souza, J.; Benet, L.Z.; Huang, Y.; Storpirtis, S. Comparison of bidirectional lamivudine and zidovudine transport using MDCK, MDCK-MDR1, and Caco-2 cell monolayers. *J. Pharm. Sci.* **2009**, *98*, 4413–4419. [\[CrossRef\]](#)

52. Luo, S.; Pal, D.; Shah, S.J.; Kwatra, D.; Paturi, K.D.; Mitra, A.K. Effect of HEPES buffer on the uptake and transport of p-glycoprotein substrates and large neutral amino acids. *Mol. Pharm.* **2010**, *7*, 412–420. [\[CrossRef\]](#)

53. Tang, F.; Ouyang, H.; Yang, J.Z.; Borchardt, R.T. Bidirectional Transport of Rhodamine 123 and Hoechst 33342, Fluorescence Probes of the Binding Sites on P-glycoprotein, across MDCK-MDR1 Cell Monolayers. *J. Pharm. Sci.* **2004**, *93*, 1185–1194. [\[CrossRef\]](#)

54. Liu, W.; Okochi, H.; Benet, L.Z.; Zhai, S.-D. Sotalol permeability in cultured-cell, rat intestine, and PAMPA system. *Pharm. Res.* **2012**, *29*, 1768–1774. [\[CrossRef\]](#)

55. Chen, C.; Mireles, R.J.; Campbell, S.D.; Lin, J.; Mills, J.B.; Xu, J.J.; Smolarek, T.A. Differential interaction of 3-hydroxy-3-methylglutaryl-CoA reductase inhibitors with ABCB1, ABCC2, and OATP1B1. *Drug Metab. Dispos.* **2005**, *33*, 537–546. [\[CrossRef\]](#)

56. Wegler, C.; Gazit, M.; Issa, K.; Subramaniam, S.; Artursson, P.; Karlsgren, M. Expanding the Efflux In Vitro Assay Toolbox: A CRISPR-Cas9 Edited MDCK Cell Line with Human BCRP and Completely Lacking Canine MDR1. *J. Pharm. Sci.* **2021**, *110*, 388–396. [\[CrossRef\]](#) [\[PubMed\]](#)

57. Simoff, I.; Karlsgren, M.; Backlund, M.; Lindström, A.-C.; Gaugaz, F.Z.; Matsson, P.; Artursson, P. Complete Knockout of Endogenous Mdr1 (Abcb1) in MDCK Cells by CRISPR-Cas9. *J. Pharm. Sci.* **2016**, *105*, 1017–1021. [\[CrossRef\]](#) [\[PubMed\]](#)

58. Ye, L.; Yang, X.; Yang, Z.; Gao, S.; Yin, T.; Liu, W.; Wang, F.; Hu, M.; Liu, Z. The role of efflux transporters on the transport of highly toxic aconitine, mesaconitine, hypaconitine, and their hydrolysates, as determined in cultured Caco-2 and transfected MDCKII cells. *Toxicol. Lett.* **2013**, *216*, 86–99. [\[CrossRef\]](#) [\[PubMed\]](#)

59. Muenster, U.; Grieshop, B.; Ickenroth, K.; Gnoth, M.J. Characterization of substrates and inhibitors for the in vitro assessment of bcrp mediated drug-drug interactions. *Pharm. Res.* **2008**, *25*, 2320–2326. [\[CrossRef\]](#)

60. Zhang, J.; Zhang, L.; Yan, Y.; Li, S.; Xie, L.; Zhong, W.; Lv, J.; Zhang, X.; Bai, Y.; Cheng, Z. Are capecitabine and the active metabolite 5-FU CNS penetrable to treat breast cancer brain metastasis? *Drug Metab. Dispos.* **2015**, *43*, 411–417. [\[CrossRef\]](#)

61. Feng, B.; West, M.; Patel, N.C.; Wager, T.; Hou, X.; Johnson, J.; Tremaine, L.; Liras, J. Validation of Human MDR1-MDCK and BCRP-MDCK Cell Lines to Improve the Prediction of Brain Penetration. *J. Pharm. Sci.* **2019**, *108*, 2476–2483. [\[CrossRef\]](#)

62. Mukkavilli, R.; Jadhav, G.; Vangala, S. Evaluation of Drug Transport in MDCKII-Wild Type, MDCKII-MDR1, MDCKII-BCRP and Caco-2 Cell Lines. *Curr. Pharm. Biotechnol.* **2018**, *19*, 1151–1158. [\[CrossRef\]](#)

63. Chen, Y.; Agarwal, S.; Shaik, N.M.; Chen, C.; Yang, Z.; Elmquist, W.F. P-glycoprotein and breast cancer resistance protein influence brain distribution of dasatinib. *J. Pharmacol. Exp. Ther.* **2009**, *330*, 956–963. [\[CrossRef\]](#)

64. Xiao, Y.; Davidson, R.; Smith, A.; Pereira, D.; Zhao, S.; Soglia, J.; Gebhard, D.; de Morais, S.; Duignan, D.B. A 96-well efflux assay to identify ABCG2 substrates using a stably transfected MDCK II cell line. *Mol. Pharm.* **2006**, *3*, 45–54. [\[CrossRef\]](#) [\[PubMed\]](#)

65. Poirier, A.; Portmann, R.; Cascais, A.-C.; Bader, U.; Walter, I.; Ullah, M.; Funk, C. The need for human breast cancer resistance protein substrate and inhibition evaluation in drug discovery and development: Why, when, and how? *Drug Metab. Dispos.* **2014**, *42*, 1466–1477. [\[CrossRef\]](#) [\[PubMed\]](#)

66. Marchetti, S.; de Vries, N.A.; Buckle, T.; Bolijn, M.J.; van Eijndhoven, M.A.J.; Beijnen, J.H.; Mazzanti, R.; van Tellingen, O.; Schellens, J.H.M. Effect of the ATP-binding cassette drug transporters ABCB1, ABCG2, and ABCC2 on erlotinib hydrochloride (Tarceva) disposition in in vitro and in vivo pharmacokinetic studies employing Bcrp1^{-/-}/Mdr1a/1b^{-/-} (triple-knockout) and wild-type mice. *Mol. Cancer Ther.* **2008**, *7*, 2280–2287. [\[CrossRef\]](#) [\[PubMed\]](#)

67. Polli, J.W.; Humphreys, J.E.; Harmon, K.A.; Castellino, S.; O’Mara, M.J.; Olson, K.L.; John-Williams, L.S.; Koch, K.M.; Serabjit-Singh, C.J. The role of efflux and uptake transporters in N-[3-chloro-4-[(3- fluorobenzyl)oxy]phenyl]-6-[5-([2-(methylsulfonyl)ethyl]amino)methyl]-2-furyl] -4-quinazolinamine (GW572016, lapatinib) disposition and drug interactions. *Drug Metab. Dispos.* **2008**, *36*, 695–701. [\[CrossRef\]](#)

68. Mahringer, A.; Delzer, J.; Fricker, G. A fluorescence-based in vitro assay for drug interactions with breast cancer resistance protein (BCRP, ABCG2). *Eur. J. Pharm. Biopharm.* **2009**, *72*, 605–613. [\[CrossRef\]](#)

69. Lau, Y.Y.; Okochi, H.; Huang, Y.; Benet, L.Z. Multiple transporters affect the disposition of atorvastatin and its two active hydroxy metabolites: Application of in vitro and ex situ systems. *J. Pharmacol. Exp. Ther.* **2006**, *316*, 762–771. [\[CrossRef\]](#)

70. Nielsen, S.; Westerhoff, A.M.; Gé, L.G.; Carlsen, K.L.; Pedersen, M.D.L.; Nielsen, C.U. MRP2-mediated transport of etoposide in MDCKII MRP2 cells is unaffected by commonly used non-ionic surfactants. *Int. J. Pharm.* **2019**, *56*, 306–315. [\[CrossRef\]](#)

71. Huisman, M.T.; Chhatha, A.A.; van Tellingen, O.; Beijnen, J.H.; Schinkel, A.H. MRP2 (ABCC2) transports taxanes and confers paclitaxel resistance and both processes are stimulated by probenecid. *Int. J. Cancer* **2005**, *116*, 824–829. [\[CrossRef\]](#)

72. Hong, L.; Xu, C.; O’Neal, S.; Bi, H.; Huang, M.; Zheng, W.; Zeng, S. Roles of P-glycoprotein and multidrug resistance protein in transporting para-aminosalicylic acid and its N-acetylated metabolite in mice brain. *Acta Pharmacol. Sin.* **2014**, *35*, 1577–1585. [\[CrossRef\]](#)

73. Zimmermann, C.; van de Wetering, K.; van de Steeg, E.; Wagenaar, E.; Vens, C.; Schinkel, A.H. Species-dependent transport and modulation properties of human and mouse multidrug resistance protein 2 (MRP2/Mrp2, ABCC2/Abcc2). *Drug Metab. Dispos.* **2008**, *36*, 631–640. [\[CrossRef\]](#)

74. Jain, R.; Agarwal, S.; Mandava, N.K.; Sheng, Y.; Mitra, A.K. Interaction of dipeptide prodrugs of saquinavir with multidrug resistance protein-2 (MRP-2): Evasion of MRP-2 mediated efflux. *Int. J. Pharm.* **2008**, *362*, 44–51. [\[CrossRef\]](#) [\[PubMed\]](#)

75. Williams, G.C.; Liu, A.; Knipp, G.; Sinko, P.J. Direct evidence that saquinavir is transported by multidrug resistance-associated protein (MRP1) and canalicular multispecific organic anion transporter (MRP2). *Antimicrob. Agents Chemother.* **2002**, *46*, 3456–3462. [\[CrossRef\]](#) [\[PubMed\]](#)

76. Tang, F.; Horie, K.; Borchardt, R.T. Are MDCK Cells Transfected with the Human MRP2 Gene a Good Model of the Human Intestinal Mucosa? *Pharm. Res.* **2002**, *19*, 773–779. [\[CrossRef\]](#)

77. Kotze, S.; Ebert, A.; Goss, K.U. Effects of Aqueous Boundary Layers and Paracellular Transport on the Efflux Ratio as a Measure of Active Transport Across Cell Layers. *Pharmaceutics* **2024**, *16*, 132. [\[CrossRef\]](#)

78. Irvine, J.D.; Takahashi, L.; Lockhart, K.; Cheong, J.; Tolan, J.W.; Selick, H.E.; Grove, J.R. MDCK (Madin-Darby canine kidney) cells: A tool for membrane permeability screening. *J. Pharm. Sci.* **1999**, *88*, 28–33. [\[CrossRef\]](#)

79. Neuhoff, S.; Ungell, A.L.; Zamora, I.; Artursson, P. pH-Dependent Bidirectional Transport of Weakly Basic Drugs across Caco-2 Monolayers: Implications for Drug-Drug Interactions. *Pharm. Res.* **2003**, *20*, 1141–1148. [\[CrossRef\]](#)

80. Heikkinen, A.T.; Mönkkönen, J.; Korjamo, T. Kinetics of cellular retention during caco-2 permeation experiments: Role of lysosomal sequestration and impact on permeability estimates. *J. Pharmacol. Exp. Ther.* **2009**, *328*, 882–892. [\[CrossRef\]](#)

81. Wang, Y.H.; Li, Y.; Yang, S.-L.; Yang, L. Classification of substrates and inhibitors of P-glycoprotein using unsupervised machine learning approach. *J. Chem. Inf. Model.* **2005**, *45*, 750–757. [\[CrossRef\]](#)

82. Tubic, M.; Wagner, D.; Spahn-Langguth, H.; Bolger, M.B.; Langguth, P. In silico modeling of non-linear drug absorption for the P-gp substrate talinolol and of consequences for the resulting pharmacodynamic effect. *Pharm. Res.* **2006**, *23*, 1712–1720. [\[CrossRef\]](#)

83. Li, C.; Liu, T.; Broske, L.; Brisson, J.-M.; Uss, A.S.; Njoroge, F.G.; Morrison, R.A.; Cheng, K.-C. Permeability evaluation of peptidic HCV protease inhibitors in Caco-2 cells-correlation with in vivo absorption predicted in humans. *Biochem. Pharmacol.* **2008**, *76*, 1757–1764. [\[CrossRef\]](#)

84. Heikkinen, A.T.; Korjamo, T.; Lepikkö, V.; Mönkkönen, J. Effects of experimental setup on the apparent concentration dependency of active efflux transport in in vitro cell permeation experiments. *Mol. Pharm.* **2010**, *7*, 605–617. [\[CrossRef\]](#) [\[PubMed\]](#)

85. Tachibana, T.; Kitamura, S.; Kato, M.; Mitsui, T.; Shirasaka, Y.; Yamashita, S.; Sugiyama, Y. Model analysis of the concentration-dependent permeability of p-gp substrates. *Pharm. Res.* **2010**, *27*, 442–446. [\[CrossRef\]](#) [\[PubMed\]](#)

86. Shirasaka, Y.; Kawasaki, M.; Sakane, T.; Omatsu, H.; Moriya, Y.; Nakamura, T.; Sakaeda, T.; Okumura, K.; Langguth, P.; Yamashita, S. Induction of human P-glycoprotein in Caco-2 cells: Development of a highly sensitive assay system for P-glycoprotein-mediated drug transport. *Drug Metab. Pharmacokinet.* **2006**, *21*, 414–423. [\[CrossRef\]](#) [\[PubMed\]](#)

87. Giddings, E.L.; Champagne, D.P.; Wu, M.H.; Laffin, J.M.; Thornton, T.M.; Valenca-Pereira, F.; Culp-Hill, R.; Fortner, K.A.; Romero, N.; East, J.; et al. Mitochondrial ATP fuels ABC transporter-mediated drug efflux in cancer chemoresistance. *Nat. Commun.* **2021**, *12*, 2804. [\[CrossRef\]](#)

88. Cox, B.; Nicolaï, J.; Williamson, B. The role of the efflux transporter, P-glycoprotein, at the blood-brain barrier in drug discovery. *Biopharm. Drug Dispos.* **2023**, *44*, 113–126. [\[CrossRef\]](#)

89. Salmina, A.B.; Kharitonova, E.V.; Gorina, Y.V.; Teplyashina, E.A.; Malinovskaya, N.A.; Khilazheva, E.D.; Mosyagina, A.I.; Morgun, A.V.; Shubaev, A.N.; Salmin, V.V.; et al. Blood-Brain Barrier and Neurovascular Unit In Vitro Models for Studying Mitochondria-Driven Molecular Mechanisms of Neurodegeneration. *Int. J. Mol. Sci.* **2021**, *22*, 4661. [\[CrossRef\]](#)

90. Ebert, A.; Goss, K.U. Blood-brain barrier permeability revisited: Predicting intrinsic passive BBB permeability using the Solubility-diffusion model. *Eur. J. Pharm. Sci.* **2025**, *215*, 107354. [\[CrossRef\]](#)

91. Benet, L.Z.; Broccatelli, F.; Oprea, T.I. BDDCS applied to over 900 drugs. *AAPS J.* **2011**, *13*, 519–547. [\[CrossRef\]](#)

92. Batrakova, E.V.; Li, S.; Elmquist, W.F.; Miller, D.W.; Alakhov, V.Y.; Kabanov, A.V. Mechanism of sensitization of MDR cancer cells by Pluronic block copolymers: Selective energy depletion. *Br. J. Cancer* **2001**, *85*, 1987–1997. [\[CrossRef\]](#)

93. Wang, J.; Seebacher, N.; Shi, H.; Kan, Q.; Duan, Z. Novel strategies to prevent the development of multidrug resistance (MDR) in cancer. *Oncotarget* **2017**, *8*, 84559–84571. [\[CrossRef\]](#)

94. Gao, X.; Aguanno, D.; Board, M.; Callaghan, R. Exploiting the metabolic energy demands of drug efflux pumps provides a strategy to overcome multidrug resistance in cancer. *Biochim. Biophys. Acta Gen. Subj.* **2021**, *1865*, 129915. [\[CrossRef\]](#)

95. Fiorillo, M.; Ózsvári, B.; Sotgia, F.; Lisanti, M.P. High ATP Production Fuels Cancer Drug Resistance and Metastasis: Implications for Mitochondrial ATP Depletion Therapy. *Front. Oncol.* **2021**, *11*, 740720. [\[CrossRef\]](#)

96. Verkman, A.S. Solute and macromolecule diffusion in cellular aqueous compartments. *TRENDS Biochem. Sci.* **2002**, *27*, 27–33. [\[CrossRef\]](#)

97. Avdeef, A. Leakiness and size exclusion of paracellular channels in cultured epithelial cell monolayers-interlaboratory comparison. *Pharm. Res.* **2010**, *27*, 480–489. [\[CrossRef\]](#) [\[PubMed\]](#)

98. Dahley, C.; Goss, K.-U.; Ebert, A. Revisiting the pKa-Flux method for determining intrinsic membrane permeability. *Eur. J. Pharm. Sci.* **2023**, *191*, 106592. [\[CrossRef\]](#) [\[PubMed\]](#)

99. Henderson, L.J. Concerning the relationship between the strength of acids and their capacity to preserve neutrality. *Am. J. Physiol.* **1908**, *21*, 173–179. [\[CrossRef\]](#)

100. Hasselbalch, K.A. Die Berechnung der Wasserstoffzahl des Blutes aus der freien und gebundenen Kohlensäure desselben, und die Sauerstoffbindung des Blutes als Funktion der Wasserstoffzahl. *Biochem. Z.* **1916**, *78*, 112–144.

101. Karlsson, J.; Artursson, P. A method for the determination of cellular permeability coefficients and aqueous boundary layer thickness in monolayers of intestinal epithelial (Caco-2) cells grown in permeable filter chambers. *Int. J. Pharm.* **1991**, *71*, 55–64. [\[CrossRef\]](#)

102. Sarkadi, B.; Homolya, L.; Szakács, G.; Váradi, A. Human multidrug resistance ABCB and ABCG transporters: Participation in a chemoimmunity defense system. *Physiol. Rev.* **2006**, *86*, 1179–1236. [\[CrossRef\]](#)

103. Dunn, J.; Grider, M.H. *Physiology, Adenosine Triphosphate*; StatPearls: Treasure Island, FL, USA, 2023.

104. Lynch, R.M.; Balaban, R.S. Energy metabolism of renal cell lines, A6 and MDCK: Regulation by Na-K-ATPase. *Am. J. Physiol. Cell Physiol.* **2019**, *252*, C225–C231. [\[CrossRef\]](#)

105. Flamholz, A.; Phillips, R.; Milo, R. The quantified cell. *Mol. Biol. Cell* **2014**, *25*, 3497–3500. [\[CrossRef\]](#) [\[PubMed\]](#)

106. Bianconi, E.; Piovesan, A.; Facchini, F.; Beraudi, A.; Casadei, R.; Frabetti, F.; Vitale, L.; Pelleri, M.C.; Tassani, S.; Piva, F.; et al. An estimation of the number of cells in the human body. *Ann. Hum. Biol.* **2013**, *40*, 463–471. [\[CrossRef\]](#) [\[PubMed\]](#)

107. Eytan, G.D.; Regev, R.; Assaraf, Y.G. Functional Reconstitution of P-glycoprotein Reveals an Apparent Near Stoichiometric Drug Transport to ATP Hydrolysis. *J. Biol. Chem.* **1996**, *271*, 3172–3178. [\[CrossRef\]](#) [\[PubMed\]](#)

108. Larisch, W.; Goss, K.-U. Calculating the first-order kinetics of three coupled, reversible processes. *SAR QSAR Environ. Res.* **2017**, *28*, 651–659. [\[CrossRef\]](#)

109. Avdeef, A.; Artursson, P.; Neuhoff, S.; Lazorova, L.; Gråsjö, J.; Tavelin, S. Caco-2 permeability of weakly basic drugs predicted with the Double-Sink PAMPA pKaflux method. *Eur. J. Pharm. Sci.* **2005**, *24*, 333–349. [\[CrossRef\]](#)

110. Mahajan, A.A.; Miniyar, P.B.; Patil, A.S.; Waghmare, R.U.; Patil, J.J.; Mohanraj, K. Separation, Identification and Characterization of Degradation Products of Erlotinib Hydrochloride Under ICH Recommended Stress Conditions by LC, LC-MS/TOF. *J. Liq. Chromatogr. Relat. Technol.* **2014**, *38*, 629–639. [\[CrossRef\]](#)

111. Budavari, S. (Ed.) *The Merck Index—Encyclopedia of Chemicals, Drugs and Biologicals*; Merck and Co., Inc.: Rahway, NJ, USA, 1989; p. 557.

112. Pailla, S.R.; Sampathi, S.; Junnuthula, V.; Maddukuri, S.; Dodoala, S.; Dyawanaipelly, S. Brain-Targeted Intranasal Delivery of Zotepine Microemulsion: Pharmacokinetics and Pharmacodynamics. *Pharmaceutics* **2022**, *14*, 978. [\[CrossRef\]](#)

113. Pfizer Canada Inc. (2016, October 28). Product Monograph: Viracept® (Nelfinavir Mesylate). Available online: https://pdf.hres.ca/dpd_pm/00037024.PDF (accessed on 1 August 2025).

114. Popović, G.; Cakar, M.; Agbaba, D. Acid-base equilibria and solubility of loratadine and desloratadine in water and micellar media. *J. Pharm. Biomed. Anal.* **2009**, *49*, 42–47. [\[CrossRef\]](#) [\[PubMed\]](#)

115. Strel'tsov, S.A.; Grokhovskii, S.L.; Kudelina, I.A.; Grokhovskii, S.L.; Kudelina, I.A.; Oleinikov, V.A.; Zhuze, A.L. Interaction of Topotecan, DNA Topoisomerase I Inhibitor, with Double-Stranded Polydeoxyribonucleotides. 1. Topotecan Dimerization in Solution. *Mol. Biol.* **2001**, *35*, 365–373. [\[CrossRef\]](#)

Disclaimer/Publisher's Note: The statements, opinions and data contained in all publications are solely those of the individual author(s) and contributor(s) and not of MDPI and/or the editor(s). MDPI and/or the editor(s) disclaim responsibility for any injury to people or property resulting from any ideas, methods, instructions or products referred to in the content.